SYNTHESIS AND STRUCTURAL CHARACTERIZATION OF BULK AND NANOALLOYS OF Ni-B BINARY SYSTEMS

A THESIS SUBMITTED TO
THE GRADUATE SCHOOL OF NATURAL AND APPLIED SCIENCES
OF
MIDDLE EAST TECHNICAL UNIVERSITY

BY

HALİM SEÇKİN TEKEKAYA

IN PARTIAL FULFILLMENT OF THE REQUIREMENTS
FOR
THE DEGREE OF MASTER OF SCIENCE
IN
METALLURGICAL AND MATERIALS ENGINEERING

JULY 2019

Approval of the thesis:

SYNTHESIS AND STRUCTURAL CHARACTERIZATION OF BULK AND NANOALLOYS OF Nİ-B BINARY SYSTEMS

submitted by **HALİM SEÇKİN TEKEKAYA** in partial fulfillment of the requirements for the degree of **Master of Science in Metallurgical and Materials Engineering Department, Middle East Technical University** by,

Prof. Dr. Halil Kalıpçılar
Dean, Graduate School of **Natural and Applied Sciences** _____

Prof. Dr. C. Hakan Gür
Head of Department, **Met. and Mat. Eng.** _____

Prof. Dr. Amdulla O. Mekhrabov
Supervisor, **Met. and Mat. Eng., METU** _____

Prof. Dr. M. Vedat Akdeniz
Co-Supervisor, **Met. and Mat. Eng., METU** _____

Examining Committee Members:

Prof. Dr. Tayfur Öztürk
Metallurgical and Materials Engineering, METU _____

Prof. Dr. Amdulla O. Mekhrabov
Met. and Mat. Eng., METU _____

Prof. Dr. M. Vedat Akdeniz
Metallurgical and Materials Engineering, METU _____

Prof. Dr. Nizami M. Gasanly
Physics Department, METU _____

Assist. Prof. Dr. Mehmet Yıldırım
Metallurgical and Materials Engineering, KTUN _____

Date: 10.07.2019

I hereby declare that all information in this document has been obtained and presented in accordance with academic rules and ethical conduct. I also declare that, as required by these rules and conduct, I have fully cited and referenced all material and results that are not original to this work.

Name, Surname: Halim Seçkin Tekekaya

Signature:

ABSTRACT

SYNTHESIS AND STRUCTURAL CHARACTERIZATION OF BULK AND NANOALLOYS OF Nİ-B BINARY SYSTEMS

Tekekaya, Halim Seçkin
Master of Science, Metallurgical and Materials Engineering
Supervisor: Prof. Dr. Amdulla O. Mekhrabov
Co-Supervisor: Prof. Dr. M. Vedat Akdeniz

July 2019, 59 pages

Nanoalloys can exhibit features which are distinct than bulk form of the same alloys. Novel properties of Ni-B magnetic nanoalloys have been used in many application areas such as; biomedicine, catalysis, nano-electronics, targeted drug delivery, data storage, magnetic separation, magnetic recording media, etc. It has been also shown that boron notably affects and increases wear resistance and hardness in nickel based alloys. Nickel based alloys having boron content show a good resistance to abrasion and galling due to boride dispersion in the structure.

This study aims to synthesize $Ni_{60}B_{40}$ alloys in the bulk and nanocrystalline-amorphous forms by means of arc melting and suction casting methods under controlled atmosphere and mechanical alloying technique, respectively and to provide comparable structural characterization of them. Initially, bulk $Ni_{60}B_{40}$ alloys were produced in equilibrium and nonequilibrium casting conditions and presence of Ni_4B_3 and Ni_2B intermetallic phases have been detected by X-ray diffractometer, SEM-EDS and DSC analysis. On the basis of DSC analysis, the melting temperatures of the Ni_4B_3 and Ni_2B crystalline phases have been founded as 1025 °C and 1142 °C, respectively, which coincide well with data published in the literature.

After the completion of structural characterization of $Ni_{60}B_{40}$ bulk alloy, milling process was performed with Nickel and Boron powders up to 80 hours of milling time. The vials were filled with Argon inert gas before milling in order to prevent oxidation. Initial sub-micron sized particles have been reduced down to a size ranged in between 50-100 nm at the end of ball milling procedure. However, microstructure of $Ni_{60}B_{40}$ nanoalloy significantly depend on milling time; amorphization of alloy starts at 40 h milling time and Ni_3B intermetallic phase starts to form at 60 h and grow with further increasing of milling time. DSC analysis of nanoalloy powders milled for 80 h milling time reveals that the $Ni_{60}B_{40}$ nanoalloy shows an amorphization behavior and glass transition and crystallization temperatures have been determined as 388 °C and 502 °C, respectively.

Also, on the basis of the particle size, it has been shown that the amount of nano-sized particles increases with further milling times. Magnetic properties of $Ni_{60}B_{40}$ bulk and nanoalloy powders have been measured by using vibrating-sample magnetometer. Magnetic measurements of $Ni_{60}B_{40}$ nanoalloys exhibit a general decrease in saturation magnetization and increase in coercivity with increasing milling time.

Keywords: Ni-B, Bulk and nanoalloys, Arc melting, High energy ball milling, Structural characterization

ÖZ

Ni-B İKİLİ SİSTEMLERİNİN HACİMLİ VE NANOALAŞIMLARININ ÜRETİMİ VE YAPISAL KARAKTERİZASYONU

Tekekaya, Halim Seçkin
Yüksek Lisans, Metalurji ve Malzeme Mühendisliği
Tez Danışmanı: Prof. Dr. Amdulla O. Mekhrabov
Ortak Tez Danışmanı: Prof. Dr. M. Vedat Akdeniz

Temmuz 2019, 59 sayfa

Nanoalaşımlar, aynı alaşımların hacimli formundan farklı olan özellikler gösterebilirler. Ni-B manyetik nanoalaşımlar biyotıp, katalizör, nano-elektronik, hedeflenen ilaç taşıyıcı, hafıza depolama, manyetik ayırma, manyetik kayıt ortamı gibi birçok uygulama alanlarında kullanılmaktadır. Ayrıca gösterilmektedir ki, nikel-boron esaslı alaşımlarda aşınma dayanımı ve sertliği önemli ölçüde etkiler ve artırır. Mikro yapı içindeki borür dağılması sebebiyle, boron içeren nikel esaslı alaşımlar aşınma ve sürtünme yapışmasına karşı iyi bir direnç gösterirler.

Bu çalışma, $Ni_{60}B_{40}$ alaşımlarını hacimli ve nano-kristal/amorf formlarında sırasıyla kontrollü atmosfer altındaki ark fırını, emme döküm metotları ve mekanik alaşımlama tekniği aracılığıyla sentezlemeyi ve onların mukayese edilebilir yapısal karakterizasyonunu sağlamayı amaçlar. İlk olarak hacimli $Ni_{60}B_{40}$ alaşımları denge ve denge dışı döküm koşullarında üretilmiştir ve Ni_4B_3, Ni_2B kristalin fazlarının varlığı X-ray kırınım, SEM-EDS ve DSC analizleriyle tespit edilmiştir. DSC analizinden yola çıkarak, Ni_4B_3 ve Ni_2B fazlarının erime sıcaklıkları sırasıyla daha önceki yapılan çalışmalarla örtüşen 1025°C and 1142°C olarak belirlenmiştir.

$Ni_{60}B_{40}$ hacimli alaşımın yapısal karakterizasyonunun tamamlanmasından sonra öğütme işlemi nikel ve boron tozlarıyla 80 saat öğütme süresine kadar

gerçekleştirilmiştir. Öğütme esnasında, oksitlenmeyi önlemek için, öğütme başlamadan önce hazneler Argon asal gazıyla doldurulmuştur. Başlangıç mikron altı boyutlu parçacıklar bilyalı öğütme işlemi sonunda 50-100 nm aralığındaki boyutlara düşürülmüştür. Bununla birlikte $Ni_{60}B_{40}$ nanoalaşımının mikro yapısı önemli ölçüde öğütme zamanına bağlıdır. Alaşımın amorfizasyonu 40 saat öğütme süresinde başlamıştır ve Ni_3B kristalin fazı 60 saat öğütme sonunda oluşmaya başlamıştır ve daha ileri öğütme süreleriyle artmıştır. 80 saat öğütme süresinde yapılan nanoalaşım tozlarının DSC analizi $Ni_{60}B_{40}$ nanoalaşımlarının amorf davranış gösterdiğini ortaya koymuştur ve camsı geçiş kristalizasyon sıcaklıkları sırasıyla 388 °C ve 502 °C olarak belirlenmiştir.

Ayrıca parçacık boyutu yönünden görülmektedir ki, nanoboyutlu parçacıkların miktarı daha ileri öğütme süreleriyle artmıştır. $Ni_{60}B_{40}$ hacimli ve nanoalaşımlarının manyetik özellikleri titreşimli örnek manyetometresi kullanarak ölçülmüştür. Manyetik ölçümler $Ni_{60}B_{40}$ nanoalaşımı için artan öğütme süreleriyle doygunluk manyetikliğinde genel bir azalış ve koersivitide ise bir artış olduğunu göstermiştir.

Anahtar Kelimeler: Ni-B, hacimli ve nanoalaşımlar, Ark ergitme, Yüksek enerjili bilyalı değirmen, Yapısal karakterizasyon

To my dear mother;

ACKNOWLEDGEMENTS

TABLE OF CONTENTS

LIST OF TABLES

LIST OF FIGURES

FIGURES

CHAPTER 1

INTRODUCTION

The features of metallic systems can be noticeably enhanced in a wide range by combining mixtures of elements to fabricate intermetallic materials and alloys. Recently, there has been a growing interest that has focused on to synthesize compounds with controllable properties on the nanometer scale [1-3].

Nanoalloys are named as clusters of atoms with size ranges between 1-100 nm. They show unique features which are shape memory effects, corrosion resistance, ferromagnetism, superconductivity, catalytic activity, structural hardness. Therefore; they are promising candidates to be utilized in many technologically important applications from electrochemical fuel and catalytic converters in automobiles to medical applications, optoelectronic and magnetic [1-6].

It is possible to generate nanoalloys in a wide range of compositions and combinations. By controlling size (p+r) and the composition (p/r) bimetallic nanoalloys may be obtained. Experimental conditions which are pressure, temperature The cluster-making method and can affect the amount of mixing or segregation and the cluster structures. Nanoalloy clusters can be fabricated in different environments including molecular beams, inside of pores, colloidal suspensions. [1-3, 7].

There are some reasons that make nanoalloys interesting. One of the significant reasons for interest is that they have additional freedom in altering properties. It means that their features can be changed by altering the composition, chemical ordering or the size of clusters. They may exhibit not only specific sizes but also specific compositions at which nanoalloys have stability.

Nanoalloys have also attracted attention because that they may exhibit distinct structures and features than elemental clusters. Besides, they may display different features than their bulk counterparts. [8-15]

1.1. Aim and Motivation

Novel properties of Ni-B magnetic nanoalloys are very useful in a wide variety of application areas, such as, biomedicine, nano-electronics, targeted drug delivery, catalysis, data storage, magnetic separation, magnetic recording media, etc. It is also shown that Boron notably affect and increase wear resistance and hardness in nickel based alloys. Nickel based alloys with boron content exhibit a good abrasion and galling resistance due to boride dispersion in the microstructure.

In this thesis, it is aimed to produce Ni-B alloys, having same composition, in the bulk and nanocrystalline/amorphous forms by means of arc melting and water cooled copper mold casting methods under controlled atmosphere and high energy ball milling technique, respectively and to provide comparable structural characterization of them. In this regard, structure, size and property relationships between them are investigated by the aid of characterization techniques.

1.2. Organization

The organization of thesis is as follows. After giving a brief introduction in the first chapter, literature review which covers definition and application of nanoalloys, Ni based alloys, Ni-B bulk and nanoalloys was given in Chapter 2. In Chapter 3, selection of composition, synthesis methods and characterization techniques of Ni-B bulk and nanoalloys were examined. In Chapter 4, the characterization results of Ni-B bulk and nanoalloys in detail with tables and figures were presented and discussed. Lastly, in the light of the findings obtained from experimental studies, conclusion was presented in Chapter 5. Beside, suggestions about potential future works were mentioned.

LITERATURE REVIEW

2.1. Nanoalloys

Nanoalloys can be categorized in terms of their mixing patterns and geometric structures

2.1.1. Mixing patterns
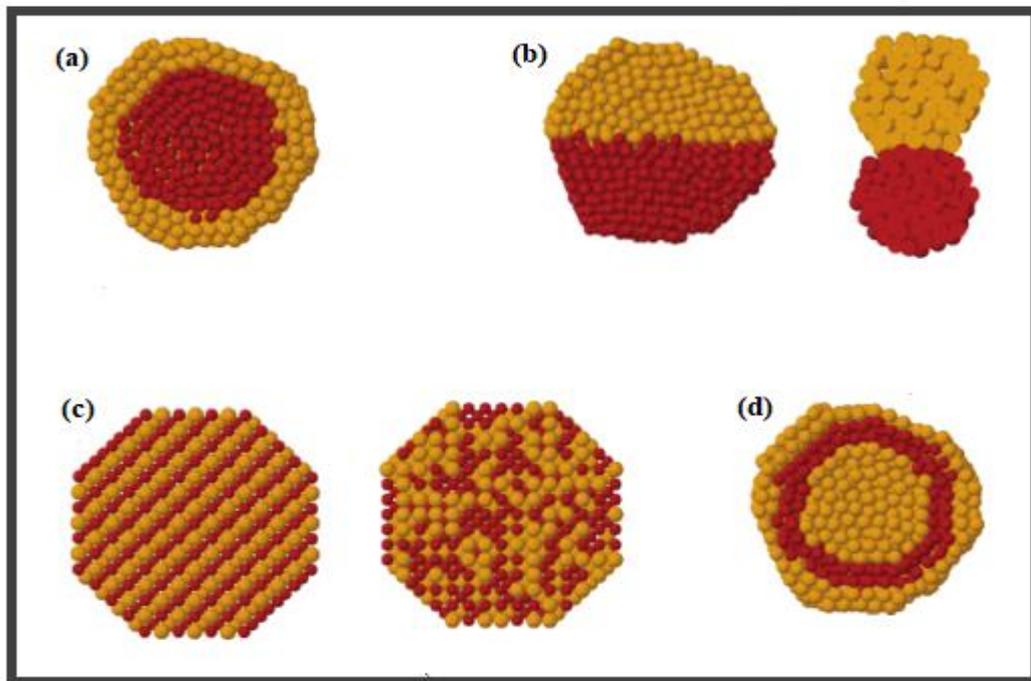
Figure 2.1 Schematic illustration of some possible mixing patterns: core-shell (a), subcluster segregated (b), mixed (c), three shell (d). The pictures exhibit cross sections of the clusters [1]

Figure 1(a) shows shell of one type of atom (B) surrounding a core of another (A). This mixing pattern is widely used in various systems. The clusters are presented $A_{core}B_{shell}$.

Figure 1(b) demonstrates A and B subclusters. They can share a mixed interface or can only possess a few number of A-B bonds. In this type, no specific examples have been found.

Figure 1(c) are ordered or random like structures. Random mixed nanoalloys are generally called as "alloyed" nanoparticles in the literature. These patterns are widespread in many systems.

Figure 1(d) are onion or layered like structures. Pd-Ag, Ni-Ag, Cu-Ag clusters are one of the examples showing this pattern in their metastable structures. Studies have also found the stable Pd-Pt and Co-Rh clusters structures for this pattern.

2.1.2. Geometric Structures

Geometric structures contain some special types demonstrated in Figure 2.2. Crystalline structures are parts of bulk crystals. Crystalline clusters may have octahedra or truncated octahedral shapes in their FCC bulk lattices. Also, non-crystalline structures which are icosahedra, decahedra, polytetrahedra, and polyicosahedra may be found.
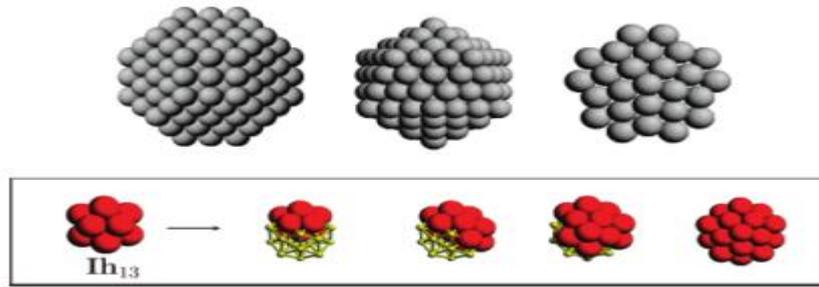
Figure 2.2 (Top row, from left to right) fcc truncated octahedron, icosahedron, and truncated decahedron. (Bottom row) Polyicosahedral cluster composed of interpenetrating elementary icosahedra of 13 atoms, here indicated by Ih13. Polyicosahedral structures are a subfamily of polytetrahedral structures because the elementary icosahedron is composed of 4-atom tetrahedral [1]

Non-crystalline structures may be found in compact shapes having an effective packing of atoms. That is provided by smaller volumes which is proportional to the strain energy between the interatomic distances so that non-crystalline icosahedra, decahedra, polytetrahedra, and polyicosahedra structures are often preferred in nanoalloys than in pure metal clusters due to smaller volume sizes. This becomes true in case of large size difference between constituent atoms as small atoms are generally located inside the cluster and decrease the compressive strain. Study on Cu-Au clusters are one of the remarkable examples for optimizing the model. The study showed that pure 55 atom Au cluster with lowest energy structure is not icosahedral. However, $Au_{54}Cu_1$ model can be created by replacing one gold atom with a copper atom to stabilize the structure.

Another study on Cu-Ag clusters with 40-atom size showed that the stability of polyicosahedral structural patterns may be enhanced thanks to electronic shell closure effects [16]. Other example can be found in 13-atom icosahedral Pb clusters that it is possible to enhance energetic stability and homo-lumo gap if an internal Pb atom is replaced by a smaller Mg atom [17].

2.1.3. Factors Affecting Ordering, Mixing and Segregation in Nanoalloys

There are some factors which influence the degree of atomic ordering and segregation/mixing in A_mB_n nanoalloys:

- Relative strengths of the A-A, A-B, BB bonds. If A-B bonds are most powerful, tendency would be mixing; otherwise, segregation is preferred. Tendency for the species constituting strongest homonuclear bonds is at the center (core) of the cluster

- Surface energies. Tendency for surface segregation is in favor of the element with lowest surface energy.

- Relative atomic sizes. Smaller atoms are more likely to be found at the sterically confined core, particularly in icosahedral clusters, where the core is subjected to compression.

- Charge transfer. Mixing is preferred when the electron changes its position from less to more electronegative elements.

- Strength of binding to surface ligands (surfactants). It is probable that, one of the elements that binds strongly to ligands tends to be on surface rather than at the core of the clusters.

- Specific electronic/magnetic effects. Stabilization of certain sizes, compositions, and/or segregation arrangements can be provided by electronic shell structure or electron spin interactions.

It should be also noted that, in addition to the balance of the factors explained above preparation method and experimental conditions are other critical parameters that should be taken into account for atomic arrangement of a specific A-B nanoalloy.

2.2. Applications of Nanoalloys

Catalysis, magnetic, optoelectronic, medical applications are some technologically important areas in which nanoalloys have already been used.

2.2.1. Catalysis

Catalytic properties of materials can be adjusted and tailored by making alloys, constituting bimetallic solids. As for nanoalloys, catalysis is one of the most utilized areas. It is possible to have remarkable catalytic properties due to surface structures, compositions, and segregation properties.

According to Schmid et. al. [18] interaction of the neighboring atoms may achieve catalytic behavior that is distinct from those of monometallic clusters due to synergistic effects. Layered (core-shell) bimetallic clusters exhibit strong perspectives in order to develop new catalysts. Bimetallic catalysts including Pt with Re or Ir have been widely used to improve petrochemicals. On the other hand, bimetallic and trimetallic clusters including Pd, Pt, and other metals have been utilized in automobile catalytic converters. Recent studies have revealed that, incorporating second element (Pt, Pd, Rh etc.) with gold (Au) to make bimetallic nanoclusters have increased the catalytic performances.

Au-Pd nanoalloys were investigated by Graham J. Hutchings et. al. [19] as redox catalysis, the small addition of Au to Pd improved the catalysis performance due to electronic effect. Methodologies for fabrication of Au-Pd nanoparticles were also discussed in this study to find best catalytic behavior on three redox reactions which are the direct synthesis of hydrogen peroxide, toluene and benzyl alcohol oxidation. While the co-impregnation technique gives the most appropriate reaction selectivity

for the direct synthesis of hydrogen peroxide and benzyl alcohol oxidation, the sol-immobilization technique provides very selective and active catalysts for toluene oxidation.

Segregation behavior of Au-Rh nanocatalysts is another example performed by Laurent Piccolo et. al. [20]. Study showed that, Au and Rh atoms immobilized on well prepared titania segregate into single-phase domains within the nanoparticles. There is no surface oxidation or sulfidation between the Rh-Au and Rh-Ti. The results also pointed out that, AuRh/TiO2 catalysts are very influential to provide the sulfidation resistance in some reactions (e.g hydrogenation of tetralin). Additionally, for hydrodeoxygenation of guaiacol AuRh catalyst showed better performances than those of Au and Rh monometallic clusters.

Recent studies have shown that, due to high cost of Au metal, less expensive ones such as; Co, Ni, Cu by alloying with Pt and Pd are favored. Ni-Pd nanoalloy catalysts utilized in the hydrogenation of nitrogen replaced aromatic compounds [21] and Ni-Pt electrocatalysts utilized in oxygen reduction in fuel cells [22] are some popular examples.

2.2.2. Magnetic Properties

There has been much recent interest for nanoalloys due to enhanced magnetic properties. Soft magnetic nanoalloys are one of important classes that can be used in various applications especially high temperature application for power generation, conversion and conditioning. The choice of the materials is very important because it is hard to find the elements with sufficiently high curry and high magnetization at high temperatures. Fe-Co nanoalloys are one of them having interesting magnetic properties. They can be used in many applications containing transformer cores, electrical motors, electrical generators, pole pieces etc. This is because they have special magnetic characteristics such as; low saturation magnetization, low coercivity, high curry temperature, high permeability etc. [23, 24]. Fe and Co based amorphous

nanoalloys have also attracted attention due to unique magnetic properties. They have a potential to be used in magnetic devices. Qi Wong et. al. [25] studied the Fe-Ni-Sb-B amorphous nanoalloys. Superior soft magnetic properties were observed from the results.

Giant magnetic resistance (GMR) is another phenomenon in which magnetic nanoalloys have been used. These GMR materials offer fascinating prospects especially they offer good prospects for utilization in magnetic recording and magnetic sensor applications. This is provided by embedding magnetic 3d metal clusters which are Fe, Ni, Co, and Cr or mixtures of these metals in a solid host containing nonmagnetic 4d (e.g., Ag, Pd, Rh) or 5d (e.g., Au, Pt) metals. Incorporating 3d metals (e.g., Ni and Co) with 4d metals (e.g., Rh) can be an efficient method to achieve high magnetic anisotropy and moment that is essential in high-density magnetic recording. Additionally, the combination of 3d metals with 5d metals can be considered as promising prospects for use in ultrahigh density magnetic recording media.

2.2.3. Biomedical Applications

As opposed to the application areas including catalysis, magnetic, there have been not many studies relating to the use of nanoalloys in biomedical applications especially in biology or medicine. This arises from limited information on the potential use of nanoalloys in that field. There have been also some concerns that are believed to influence the utilization of nanoalloys. Toxicity and biocompatibility are one of the main concerns that should be considered. As it is known that, certain materials are toxic in the bulk form. To The Occupational Safety and Health Administration of the Department of Labor, arsenic (As), beryllium (Be), cadmium (Cd), lead (Pb) and mercury (Hg) are accepted as toxic metals. Active metals like Ti, Zr, and Nb may be biocompatible due to passive biocompatible oxide. Spontaneous formation and stability of this passive oxide determine the biocompatibility of the alloys. Additionally, metals or alloys with size in the nanometer can exhibit different biocompatible behavior than those of their bulk counterparts. While noble metals such

as gold (Au), platinum (Pt), palladium (Pd) and silver (Ag) are widely known as biocompatible, Ag nanoparticles can be highly active and release Ag ions that can be possibly toxic [26].
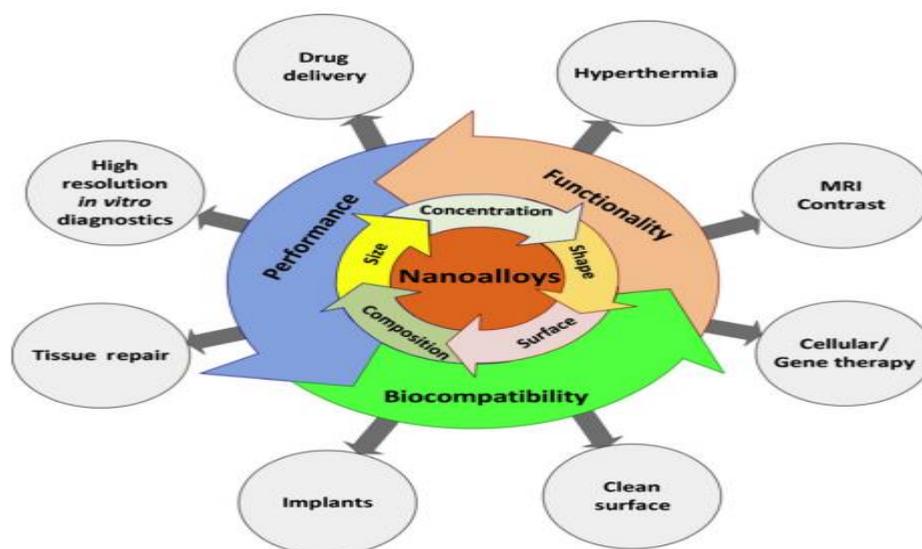
Figure 2.3 A summary of physiochemical considerations important for potential biomedical applications of nanoalloys [26]

Magnetic bimetallic nanoparticles are of interest due to unique properties. They can exist in many applications containing magnetic separation, data storage, magnetic recording media, sensors and biomedicine. There have been some researches on Fe-Pt and Fe-Co magnetic bimetallic nanoparticles which are good candidates for biomedical applications. Fe-Pt and Fe-Co possess high saturation magnetizations and can be beneficial in biomedical applications such as MRI contrasts and drug delivery. However, the key problem is that there has been no information on biocompatibility and cytotoxicity of these materials.

2.2.4. Other Application Areas

With the development of well defined, controlled synthesis methods, nanoalloys can be utilized in other application areas. It is anticipated that, the use of nanoalloys will be extended in a wide range of applications. According to some projections future is bright for development of new technologically important areas where nanoalloys will be used. For example, constructions of 1D, 2D, and 3D nano-architectures can take place in coming years with the development of technology. In addition to this, it is predicted that, the use of tri- and multi-metallic nanoalloys with heterogeneous particles which are alloy-oxide composites and functionalized hybrid bio-nanoalloy particles for medical application areas is developed in the future.

2.3. Mechanical Behavior of Nanocrystalline Metals and Alloys

There are some methods in which nanocrystalline and ultrafine crystalline materials are synthesized. Mechanical alloying, severe plastic deformation electrodeposition and gas phase condensation are some of the main production techniques. The studies have demonstrated that different mechanical properties can be achieved by these methods.

K. S. Kumar et al. [27] investigated the nanocrystalline metals and alloys in terms of mechanical properties. The objective of this paper was to examine the structural characterizations of nanocrystalline metals and to investigate the mechanisms underlying mechanical response using experimental tools and computational simulations. It was concluded from the experimental and computational results that, grain boundaries play a significant role in considering the structure of nanocrystalline metals and alloys and its influence on deformation behavior. Grain boundaries in nanocrystalline metals and alloys are significantly analogous with those of microcrystalline counterparts. However, it was not still clear to set up a connection between the structure and mechanical properties. Findings in experimental studies

were not enough to support the computational simulations so that it was required to connect between the experimental and computational studies.

2.4. Nickel Based Alloys

The utilization of nickel dates back to the beginning of civilization. Researches have demonstrated that various amount of nickel was utilized in a wide variety of objects in the past. The uses of nickel in elemental form or alloyed with other metals and materials have extended to a diverse range of application areas at the present time and continue to supply materials for future. One of the main purpose of nickel is to generate alloys.

Ni based alloys demonstrate excellent resistance wear and corrosion resistance like Ni. Due to physical properties, Nickel alloys may be used in applications that need high wear resistance, magnetic properties, and high strength particularly at high temperatures. There are some main applications of Ni and Ni based alloys as follows:

• Chemical and marine industries: valves, fans, bolts, tubing, reaction vessels, pumps, transfer piping.

• Pulp and papermills: tubing, bleaching circuit equipment, doctor blades, scrubbers.

• Making gas turbines: disks, shafts, combustion chambers, bolts, casings, exhaust systems, vanes, blades.

• Steam turbine power plants: bolts, blades, stack gas reheaters.

• Reciprocating engines: Exhaust valves, turbo chargers, valve seat inserts. hot plugs.

• Metal processing: dies and hardwork tools.

• Medical applications: dentistry uses, prosthetic devices.

• Space vehicles: rocket engine parts, aerodynamically heated skins [28].

Nickel may be also utilized to obtain protective coating on the substrate metal. The nickel plating process is one of the coating process that is extended to a diverse range of applications which are decorative, engineering and electroforming. Electroless nickel coatings are obtained by the autocatalytic chemical reduction of nickel ions from an aqueous solution. There are three kinds of electroless coatings: nickel-boron (~5% B), nickel-phosphorus (6 to 12% P) and composite coatings. These coatings are important to prevent materials from corrosion and wear. As for thermal spray coatings, alloys including nickel-chromium carbide, nickel-chromium boride and nickel tungsten carbide are used for wear resistance in applications. Weld-overlay coatings are another method that is utilized for wear resistant (hardfacing alloys) and corrosion resistant applications (weld claddings). Ni based alloys are presented in other fields due to their excellent physical properties with shape memory, low expansion, soft magnetic, etc. [28].

2.5. Ni-B Bulk Systems

There have been a number of researches which is related the use of boron as an essential alloying element in many nickel alloys. For hardfacing applications, the thermal spraying is a process in which boron containing nickel alloys have been used. With the addition of boron, the melting point of Nickel can be reduced and it allows to produce hard and dense coatings. The other important feature of boron is that it can form borides with high hardness in ternary alloys [29].

J. Diabb et al. [30] investigated influence of boron on wear resistance in nickel based alloys. The purpose was to examine the wear and hardness behavior of the ternary Ni-B-Si alloys. Results demonstrated that, Ni_3B intermetallic increased with the increase of Boron and hardness and wear resistant showed an important increment.

L. Xi, I. Kaban et al. [31] studied the Ni-B Alloys for Joining of TiB_2. Melting and wetting properties of Ni-B alloys on TiB_2 ceramic were investigated for the application in ceramic joining. The purpose was to examine the development of desired joints without defects and satisfying strength was aimed for potential use in

engineering applications. It was concluded that $Ni_{50}B_{50}$ alloy was well bonded to TiB_2, promising to be used in high temperature applications (aerospace, automotive, and defense).

As for coating applications, Ni-B coatings can be seen as good candidate in various industrial applications. They provide cost effectiveness, high hardness, low wear, lubricity, uniform thickness, good ductility, excellent solderability, corrosion resistance and antibacterial activity. Electroless Ni-B coatings on pure titanium surface was researched by F. Mindivan et al. [32]. According to results, electroless Ni-B coated on pure titanium showed better hardness, tribocorrosion and antimicrobial activity performance than pure titanium. The other study on electroless Ni-B coatings was done by Ferhat Bulbul et al. [33]. The 316L stainless steel was chosen as substrate material. Improvement of the modest mechanical properties (poor fatigue and wear resistance) of the 316L stainless steel was aimed applying the electroless Ni-B coatings. It was concluded from the study that 316L stainless steel exhibited better hardness and wear resistance behavior and also cathodic protection was attained by protecting the original features of the 316L stainless steel.

Ni-B thin films also has also drawn much attention owing to unique properties. A. Glass et all. [34] studied the Ni-B thin films obtained from borane and metallaborane compounds. Various Ni-B thin film compositions having different sizes were attained and subjected to characterization processes which are SEM, XES and AES. Results demonstrated that, the Ni-B thin film alloys with soft magnetic features have a huge potential to be used in the field of high magnetic recording. Beside, susceptibilities of different sized Ni-B thin films at room temperature were examined. Susceptibility values increased with the decrease of particle sizes. According to researchers, the reason behind these differences was related to the magnitude of defects occurring on them.

2.5.1. Phase diagram of the Ni-B System
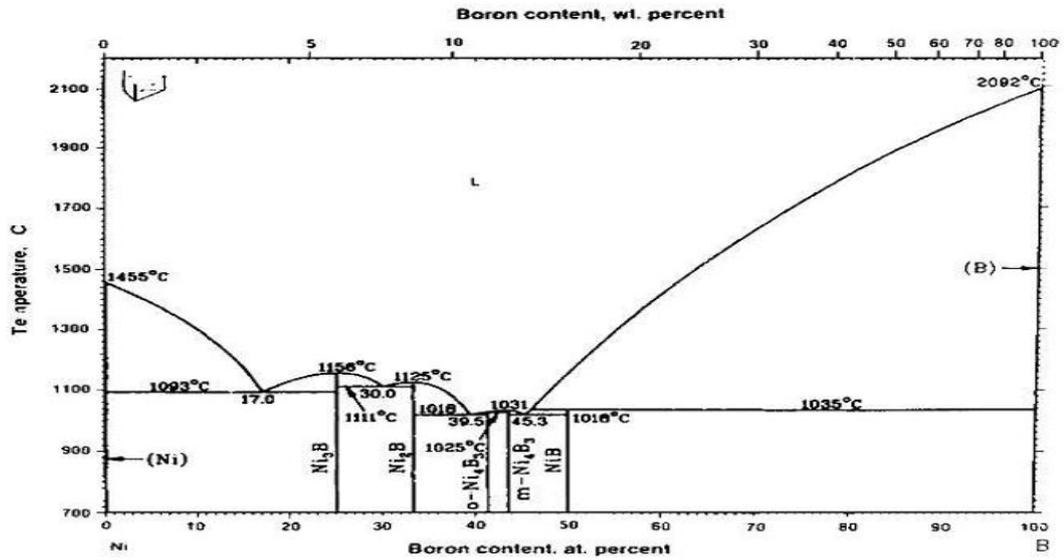
Figure 2.4 Ni-B Phase Diagram [35]

As seen in Figure 2.4, four eutectic compositions possible and five intermetallic compounds exist in the Ni-B phase diagram. Crystallographic data of Ni-B system containing the intermetallics are indicated in Table 2.1

Table 2.1 Crystallographic data of Ni-B binary system [29]

Phase	Structure	Type
(Ni)	Face Centered Cubic	Cu
Ni3B	Orthorhombic	CFe3
Ni2B	Tetragonal	Al2Cu
Ni4B3(o)	Orthorhombic	B3Ni4
Ni4B3(m)	Monoclinic	B3Ni4
NiB	Orthorhombic	BCr
(B)	Rhombohedral	B

15

These intermetallics take place in several interesting applications which are electroless coatings, brazing filler metals, thin/thick films, and master alloys thanks to their novel properties containing low melting point compared to elemental constituents, super wear and corrosion resistance, strong electrical conductivity, better catalytic characteristics [36-38]. Additionally, they may be substituted for such noble metals such as; Pd, Ag, and Au in some electronic applications owing to their attractive properties and lower cost. Moreover, nickel borides catalysts have successfully been utilized for hydrogen generation [39-41].

There have been some researches on the Ni-B phase diagram. From thermodynamic perspective, Ni-B phase diagram was assessed by O. Teppa et al. [37]. An optimization technique was carried out to all thermodynamic data providing internally consistent thermodynamic model parameters and coefficients. Gibbs energies of the intermetallic phases obtained was compatible with experimental results.

Stig Rundqvist et al. [42] calculated the interatomic distance of Ni_3B, o-Ni_3B and m-Ni_4B_3 crystal structures using three-dimensional intensity material which is different from the previous methods. Results showed that, due to noticeable improvement of boron parameters, Ni-B and B-B distances obtained from the three dimensional intensity materials was more reliable than the previous values.

There have been also some studies on Ni-B amorphous alloys due to their good selectivity, high catalytic activity and strong sulfur resistance in many hydrogenation reactions. S. Diplas et al. [43] characterized the Ni-B amorphous alloy catalysts produced by electrodeposition method for potential utilization in hydrogen energy applications.

Inoue et al. [44] studied the Ni-B amorphous alloys having high boron concentration. Formation of the Ni based binary amorphous alloys for Ni-B system was carried out by rapid quenching from their liquid state and compositions were restricted to range

16

of 33-43 at % B. Vickers hardness (H_V), crystallization temperature (T_x), fracture strength (σ_f), and critical fracture temperature (T_f) of amorphous Ni- B alloys were calculated as it is shown in Table 2.2.

Table 2.2 Vickers hardness (H_V), fracture strength (σ_f), crystallization temperature (T_x) and critical fracture temperature (T_f) of amorphous Ni-B alloys [43]

Alloy system (at%)	Vickers hardness, H_v (DPN)	Fracture strength σ_f (MPa)	Crystallization temperature, T_x (K, 8.33×10^{-2} K/s)	Critical fracture temperature, T_f (K, $\times 6000$ s)
$Ni_{66}B_{34}$	685	2480	658	650
$Ni_{64}B_{36}$	760	2370	662	640
$Ni_{62}B_{38}$	810	—	659	640
$Ni_{60}B_{40}$	850	3410	663	590
$Ni_{58}B_{42}$	865	—	655	—

Campbell et al. [45] reported the amorphous Ni-B alloy formed through solid state and ion-beam reaction. It was obtained between layers of polycrystalline nickel and amorphous boron. Results showed that, amorphous Ni–B alloy layer reached maximum thickness value (40 nm) during the electron beam deposition of Ni-B-Ni trilayer structures. This layer obtained in the structure was the indication of a reaction barrier but further increase of thickness was not accomplished through the production method.

The hydrogen activity of different boron containing Ni-B amorphous alloys was investigated by Hui et al. [46]. Two compositions ($Ni_{67.3}B_{32.7}$ and $Ni_{95.2}B_{4.8}$) with different B content were compared in terms of hydrogen activity. It was attributed to both structural and electronic effect. In terms of structural effect, $Ni_{67.3}B_{32.7}$ with more stable amorphous structure showed better catalytic activity owing to promoting effect

of B. As for electronic effect, high amount of B enhanced the catalytic activity of amorphous structure, making Ni active sites more electron enriched.

2.6. Ni-B Nanoalloy Systems

There has been a growing interest on crystalline/amorphous nanoscale Ni-B materials for potential use in the field of catalysis, hydrogen storage and magnetic recording applications [47-54].

Yi Wang et al. [55] investigated the Ni-B nanoalloy doped 2D graphene for potential hydrogen storage applications. Chemical reduction method was used for doping of 2D graphene material with Ni-B nanoalloys. The doping of 14 wt.% Ni and 0.63 wt.% B on the graphene significantly increased the hydrogen storage capacity which is more than that of 2D graphene. It can be concluded that, Ni-B nanoalloys can be a good candidate as catalyst for hydrogen spillover application on graphene.

Firoozeh Taghavi et al. [56] kinetically studied the nano-Ni_2B catalyst particles in terms of catalytic activity for hydrogenation. The influence of reaction temperature, initial concentration and pressure on the reaction kinetics were examined. According to results, while the increasing of reaction temperature and initial concentration enhanced the reaction rate, increasing of pressure decreased the reaction rate. Additionally, the catalytic activity of these nano-Ni_2B catalyst particles were compared to Raney nickel. Experiments were carried out under same conditions. The Ni_2B catalyst exhibited better performance owing to boron electron donation in the structure.

Hong-Beom Kwon et al. [57] reported the nanocrystalline Ni-B with low boron content via electrodeposition method and characterized it in the field of microelectromechanical systems (MEMS) that need high mechanical performance. Production was carried out by electrodeposition in a nickel sulfamate solution, arranging the concentration of the boron source, dimethyleamine borane (DMAB). The mechanical properties of nanocrystalline Ni–B electrodeposits were considerably

increased and they showed outstanding mechanical performance. The hardness and elastic modulus of Ni–0.19B with 573 K heat treatment were higher than those of pure nanocrystalline Ni.

Lei Xu et al. [58] studied the Ni-B amorphous nanoparticles obtained from aqueous reduction method. As a result of the experiment, nanoparticles produced showed amorphous structure. It was presented in XRD patterns that all the specimens showed amorphous structure. Also, average particle diameter size reduced down to 9 nm. In terms of morphological examination, synthesized Ni-B amorphous nanoparticles were spherical and showed a good dispersion.

Zheng Jiang et al. [59] investigated the nano-amorphous Ni-B alloys in terms of both structure and catalytic properties. Chemical reduction method was used to synthesize Ni-B amorphous nanoalloys and benzene hydrogenation was preferred to observe the catalytic activities of the nano-amorphous Ni-B catalysts annealed at different temperatures. At 623 K, Ni-B amorphous nanoalloys showed better catalytic activity, reaching the maximum benzene conversion and turnover frequency values. However, it decreased at higher annealing temperatures. The reason was attributed to the formation of various phases occurring at different annealing temperatures. Nanocrystalline Ni and crystalline Ni_3B phases forming at 623 K showed the highest degree of catalytic activity. With the increasing temperature, it decreased due to different structure with less catalytic phases.

The non-noble metals have been investigated in numerous studies for potential use in the field of catalytic applications. due to low cost, high abundance, high catalytic performance, corrosion resistance non-noble metals may be replaced with noble metals like Pt group metals in the future. One of the researches related to this was published by Min Zeng et al. [60]. The research was on hydrogen evolution reaction activity of nanostructured amorphous nickel boride. Electroless plating method was used to fabricate Ni-B catalyst. According to experimental results, it showed outstanding catalytic efficiency and long term stability compared to Pt. This high

catalytic activity was attributed to the amorphous and electronic effect. To conclude that, amorphous Ni-B may be excellent candidate for the replacement of noble metals.

Vidyadhar Singh et al. [61] investigated the Ni rich amorphous boride nanoparticles in terms of structural and magnetic features. They were obtained by the solid-solid reaction of the $NiCl_2$ and $NaBH_4$ powders in ambient conditions. XRD, FESEM, TEM, DTA-TG, and DC magnetization techniques were used for characterization of synthesized powders. Results exhibited that the fabrication of the Ni rich amorphous boride nanoparticles was prepared successfully using the solid-solid reaction technique which is simple and cost effective. Magnetic properties of the Ni rich boride NPs were completely distinct from those of the poly-crystalline and ribbon samples. As-prepared Ni rich boride nanoparticles exhibited a very low Hc value indicating the superparamagnetic properties at room temperature.

Korchagin et al. [62] studied the production of nickel boride using high energy ball milling. Development of formation route of Ni_3B phase was aimed in this study. Totally 15 minutes of milling time with certain intervals was carried out for powder mixtures. Results indicated that, with the increase of milling time boron dissolved into Ni and crystallite sizes decreased. Also, heating of the mixtures resulted in thermal explosion which indicates the occurrence of Ni_3B phase and rapid increase of temperature. The maximum temperature was determined at 1 hour of milling time then decreased with further milling times, reaching the level of the non-milled conditions at the end of the process. The decrease of temperature was attributed to the structural transformations in the mixture.

A. Corrias et al. [63] studied the fabrication of nanocrystalline sized nickel boride powders. Starting from the micrometer sized elemental components mechanical alloying was applied to $Ni_{60}B_{40}$ and $Ni_{80}B_{20}$ mixtures Mechanical alloying of powders was performed in a planetary Fritsch Pulverisette 5 ball mill. Solid state reactions of the mixing of components were examined through milling process. According to results although the time evolution of the reaction showed similarities in the two

20

samples final products of both compositions were not similar. Reactions started with the appearance of o-Ni$_3$B in both compositions then changed with the increasing milling times. At the end of the process, o-Ni$_3$B crystalline phase and unreacted Ni formed in Ni$_{80}$B$_{20}$ composition while t-Ni$_2$B crystalline phase formed in Ni$_{60}$B$_{40}$.

T. Nasu et al. [64] published an article about solid state amorphization of Ni-B nanoalloy through mechanical alloying. Possible formation of solid state amorphization was investigated as a means of X-ray diffraction and EXAFS characterization methods. The amorphization reaction was observed in Ni$_{64}$B$_{36}$ at 400 h of milling time and rise of the dissolution of B atoms into the Ni matrix led to decrease of the long range order of Ni phase. This indicated that dissolution of B atoms into the Ni crystalline has an impact on the crystal amorphous transformation.

Another study on mechanical alloying method was done by Masoud Nazarian-Samani et al. [65]. DTA and detailed XRD methods were combined to analyze the mechanically alloyed Ni–15 wt. % B in high energy ball milling. Evolution of phases was studied in terms of thermodynamic perspective. Nanocrystalline Ni–B alloys composed of Ni$_2$B + o-Ni$_4$B$_3$ and Ni$_2$B + m-Ni$_4$B$_3$ + B were formed by different phase transition sequences. According to XRD results the Ni$_2$B intermetallic phase showed the highest stability in the Ni–B binary phase diagram, and no change was observed in its nanocrystalline nature even after high annealing temperatures which are near the melting point. Furthermore, average enthalpy and activation energy of reaction forming during the process were determined.

There are numerous methods to generate Ni-B nanoalloys ranging from, chemical reduction, molecular beams, ion implantation to thermal decomposition of transition-metal complexes, electrochemical synthesis, mechanical alloying by high energy ball milling etc. In this thesis, for the generation of Ni-B nanoalloys, mechanical alloying by high energy ball milling technique was used.

2.7. Mechanical alloying by high energy ball milling

Mechanical alloying (MA) is one of the powder processing technique that allows to produce nanocrystalline/amorphous alloys, extended solid solutions, metastable crystalline phases, quasicrystals etc. [66-79]. It is a simple, low cost method that enables to eliminate problems such as large difference in melting points of the alloying components as well as undesired segregation or evaporation that can form during melting and casting. In the MA process, right proportion of powder materials and milling balls are placed together in a milling bowl then milling process starts with strong vibrational or rotational acceleration [80, 81].
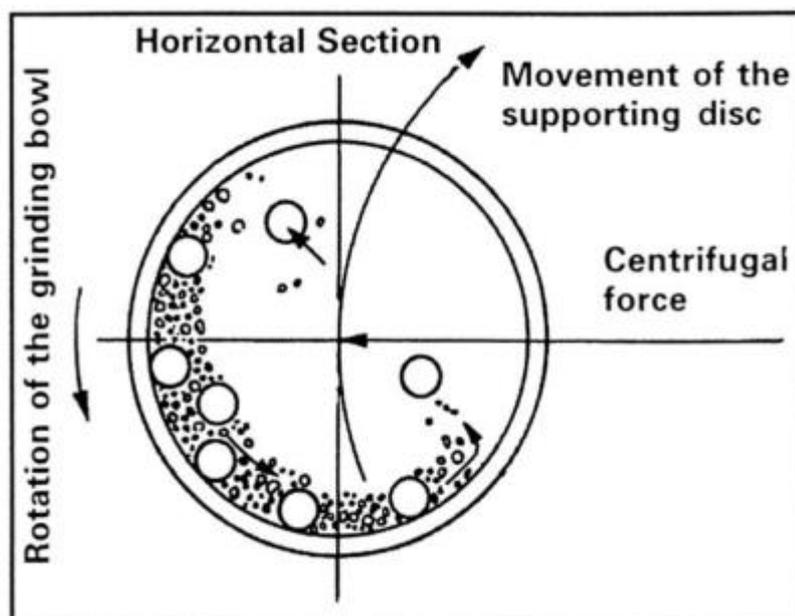
Figure 2.5 Schematic view of ball and powder mixture [81]

During the milling process, powder particles are trapped between the milling balls. With the collision of the balls, powders are exposed to repeated plastic deformation, fracturing and cold welding. In this technique, as particle size decreases, milling operation generates micro-deformation of the crystal lattice of the ground material.
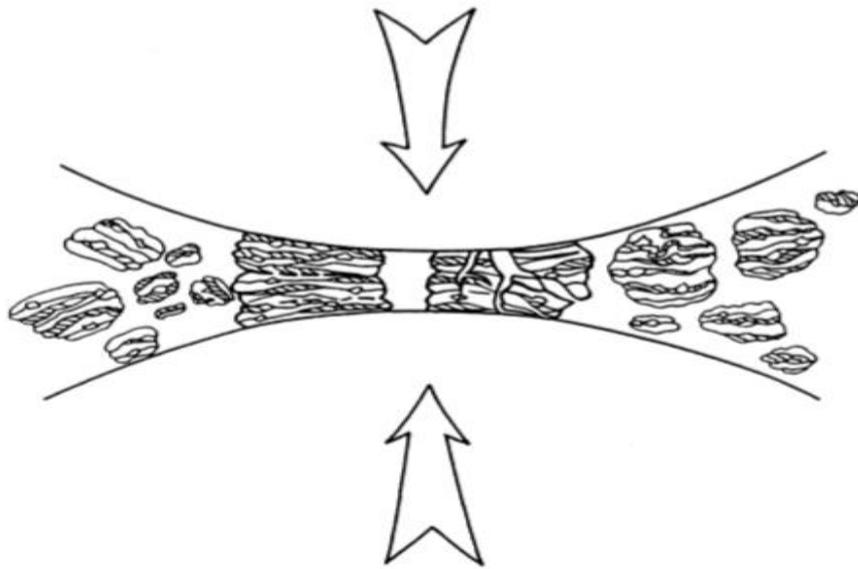
Figure 2.6 Ball-powder-ball collision of powder mixture during mechanical alloying
[81]
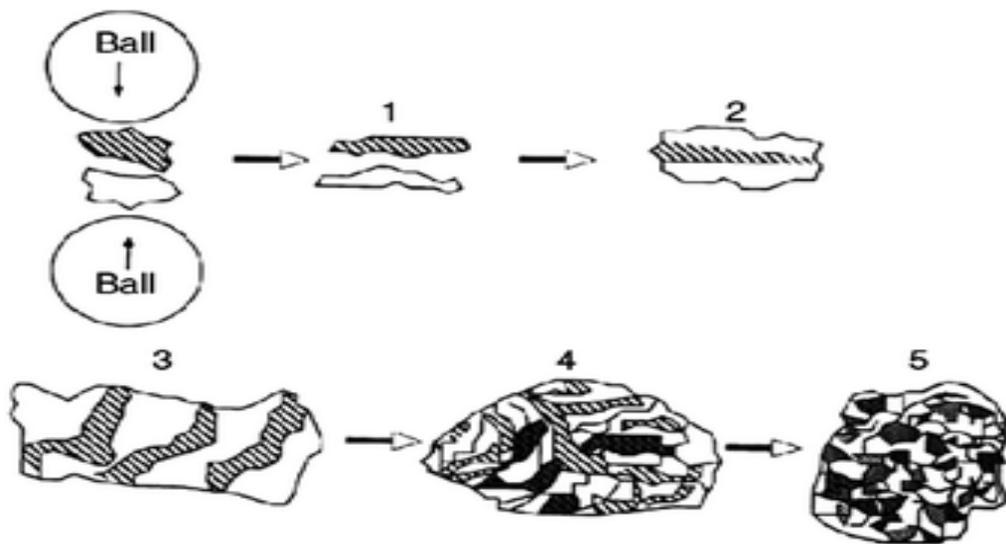
Figure 2.7 Evolution of different stages of mechanical alloying [81]

Mechanical alloying is a complex process and therefore includes optimization of a number of variables to attain the desired product phase and/or microstructure. There are some important parameters influencing the final constitution of the powder:

- type of mill,
- milling container,
- milling speed,
- milling time,
- milling temperature
- type, size, and size distribution of the grinding medium,
- ball-to-powder weight ratio,
- extent of filling the vial,
- milling atmosphere,
- process control agent

CHAPTER 3

EXPERIMENTAL PROCEDURE

3.1. Selection of Ni-B bulk alloys composition
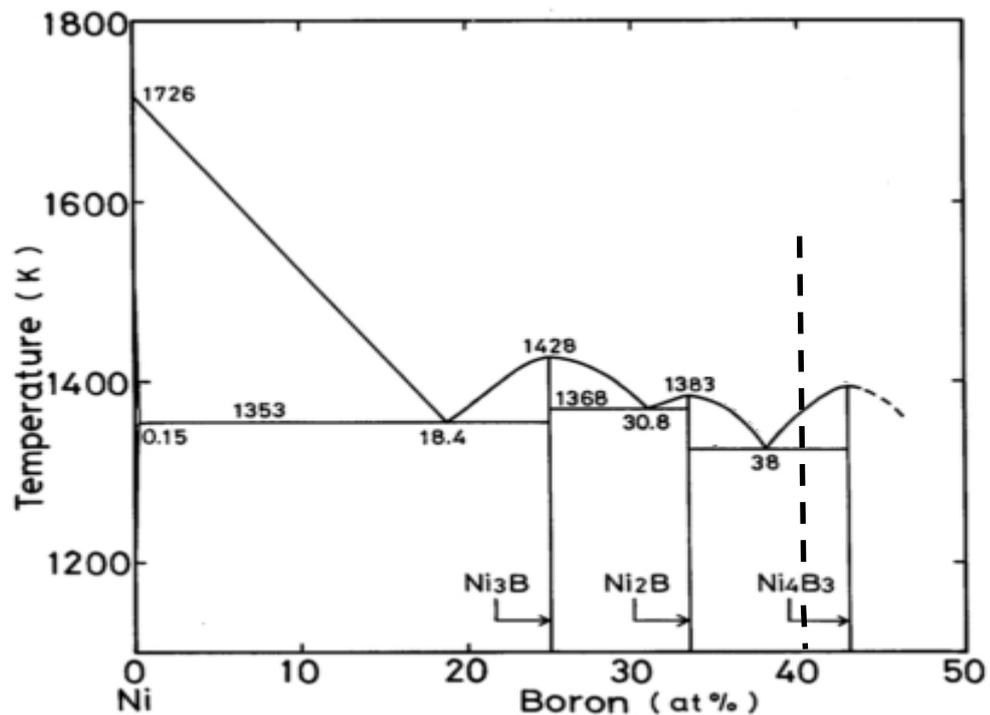
Figure 3.1 Partial phase diagram of Ni-B binary system [44]

The composition of Ni-B bulk alloys was determined as $Ni_{60}B_{40}$ which corresponds to the hypereutectic point in Ni-B phase diagram. Owing to their excellent mechanical properties mentioned previously in literature section, Ni-B intermetallic compounds offer good prospects for potential use in many application areas. Numerous researches have focused on the synthesis and characterization of these intermetallics. The composition selected in this thesis exist between two intermetallics which are Ni_2B

and Ni_4B_3. Also, possible formation of Ni_3B intermetallic phase was considered during the arc melting and suction casting process.

Table 3.1 Purities of alloying elements (wt.%)

Element	Grade (wt.%)
Ni	99.5
B	99.5

3.2. Synthesis of $Ni_{60}B_{40}$ bulk alloys

The $Ni_{60}B_{40}$ bulk alloys were synthesized by arc melting unite using a water- cooled copper hearth and non-consumable tungsten electrode under high purity argon atmosphere. Zr was located in the chamber to reduce oxygen during the melting process. Moreover, diffusion and rotary pumps supplied oxygen free and an ideal melting atmosphere that is important to prevent bulk alloy mixture from the adverse effect of oxygen. Then mixture of alloying elements was melted in oxygen free/inert argon gas environment. Homogeneity was achieved by remelting samples three times.

Figure 3.2 Arc melting unit used for the production of samples

After arc melting processes, molten $Ni_{60}B_{40}$ bulk alloys were sucked into the copper mold by using pressure difference between the melting chamber and the casting chamber. $Ni_{60}B_{40}$ cylindrical bulk alloy rod with diameter of 3 mm was obtained at the end of the suction casting process.

Figure 3.3 Copper mold and cylindrical $Ni_{60}B_{40}$ bulk rod.

3.3. Synthesis of $Ni_{60}B_{40}$ Nanoalloys

In this thesis, The ball milling equipment depicted in Figure 3.4 was used for milling process.

Figure 3.4 Fritsch Pulverisette 7 Premium Line High Energy Ball Mill, stainless steel bowl / balls and Ni-B powder mixture

In this experiments, type of mill, type of bowl, volume of bowl, ball to powder ratio, milling time, milling atmosphere were taken into consideration as critical parameters in determining the final properties of powders. Moreover, during high energy ball milling experiments, it was very important to protect equipment from overheating and excess pressure within the bowls so cooling time was selected thoroughly.

3.3.1. Milling parameters of pure Ni powder and $Ni_{60}B_{40}$ powder mixture

Before starting the milling process of $Ni_{60}B_{40}$ powders, in order to comprehend the mechanism of the high energy ball milling and to analyze the effect of milling parameters including rotation speed, milling time, type of bowls and balls, ball to powder ratio etc. Milling operation was applied to high purity Ni powders (99.5 wt. %, 48 μm). Stainless steel bowls (each 20 ml) and each of balls with 5mm in diameter and 0.51 gr in weight were utilized for grinding process. In addition, ball to powder ratio was selected as 10:1. Totally 4 g Ni powders were loaded in each of stainless steel bowls with 40 g stainless steel balls. In order to protect Ni powders from oxidation, Ar gas was transferred into bowls at a pressure about 1 bar before milling. Speed of rotation was decided as 250 rpm and milling process was carried out in 15 minutes grinding cycles. After each 15-minute cycle, in order to protect equipment from overheating, equipment was left to cool down for 15 minutes. After 1, 5, 10, 20 h milling times, powders were taken from the bowls for characterization. Total milling process was performed up to 20 hours of milling time. After finishing the characterization of pure Ni powders, the milling process of $Ni_{60}B_{40}$ powder mixtures started. Same milling parameters were defined. Totally, 80 hours of milling time was applied to powder mixture. The milling parameters of both pure Ni and $Ni_{60}B_{40}$ powders were determined according to the previous studies at NOVALAB [82, 83].

3.4. Characterization of Samples

3.4.1. X-ray Diffraction (XRD)

Phase analyses of as cast $Ni_{60}B_{40}$ bulk and nanoalloys were carried out by X-ray diffraction method using Bruker D8 Advance with Cu-Kα radiation (λ = 1.5418 Å) for the angle range of 2θ = 20° – 120° with a scanning rate of 2°/minutes.

3.4.2. Scanning Electron Microscopy (SEM)

FESEM was used for the microstructural characteristics of as cast $Ni_{60}B_{40}$ bulk alloys and milled Ni-B nanoalloys. For characterization of $Ni_{60}B_{40}$ bulk alloys, cylindrical rod was cut into little pieces then most suitable one (3 mm diameter and 2 mm height) was selected. After finishing the metallographic process, piece was loaded in SEM equipment for characterization. For $Ni_{60}B_{40}$ nanoalloys, the adequate amount of Ni-B powders mixture (approximately 10 mg) were put on the aluminum sample holder, then holders were placed into SEM equipment for characterization.

3.4.3. Differential Scanning Calorimetry (DSC)

DSC was utilized to observe the amount of energy absorbed or released by the specimen after heating or cooling with endothermic and exothermic processes. In this study, samples of 15-20 mg weight were put into alumina crucibles then placed into DSC equipment depicted in Figure 3.5. Sample was heated up to 1250 °C at a constant heating rate of 20 °C, then was cooled to room temperature constant cooling rate of 20 °C. After first heating-cooling stage, second heating-cooling stage was performed to obtain more stable structure under equilibrium condition.

Figure 3.5 Differential Scanning Calorimeter (DSC) Setaram Setsys 16/18

3.4.4. Vibrating Sample Magnetometer (VSM)

Magnetic calculations of samples were performed with VSM device depicted in Figure 3.6. Calculations were carried out at room temperature.
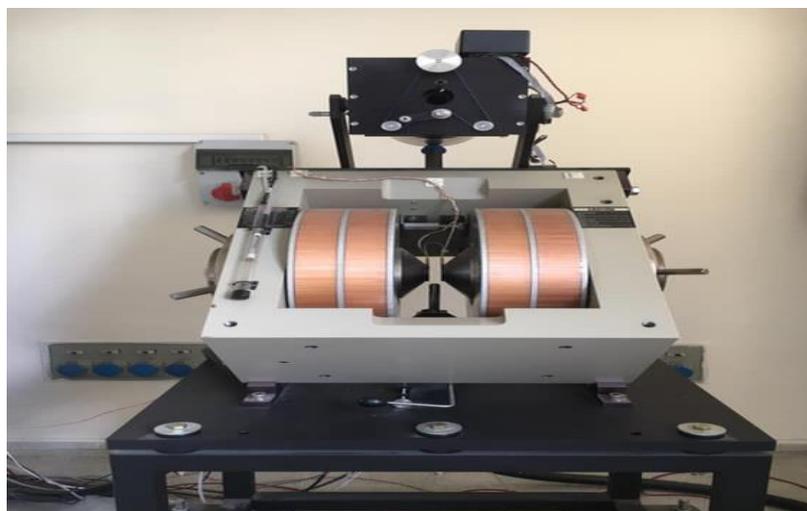
Figure 3.6 ADE Magnetics EV/9 Vibrating Sample Magnetometer (VSM) under a maximum applied field of 18000 Oe.

CHAPTER 4

RESULTS AND DISCUSSIONS

4.1. Characterization of as-cast $Ni_{60}B_{40}$ bulk alloys

After finishing the metallographic treatments, the characterization techniques were applied to sliced piece of the $Ni_{60}B_{40}$ bulk rod alloy. Figure 4.1 shows the XRD patterns of $Ni_{60}B_{40}$ bulk alloy sample obtained by the suction casting method. As seen from the graph two crystalline phases of Ni_2B (tetragonal) and Ni_4B_3 (orthorhombic) are presented.
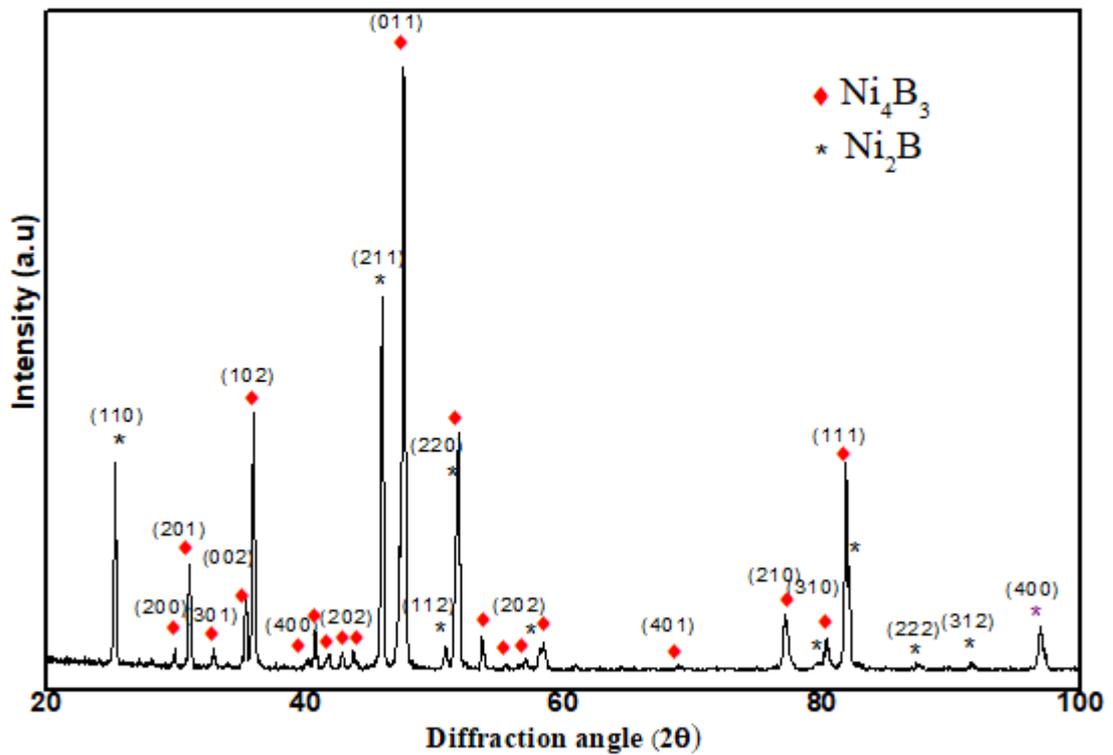
Figure 4.1 X-Ray diffraction patterns of $Ni_{60}B_{40}$ bulk alloy rod

After XRD analysis, SEM analysis was carried out for further classification of phases presented in the microstructure, Fig. 4.2 pro-eutectic and eutectic intermetallic phases are evident in the SEM image.
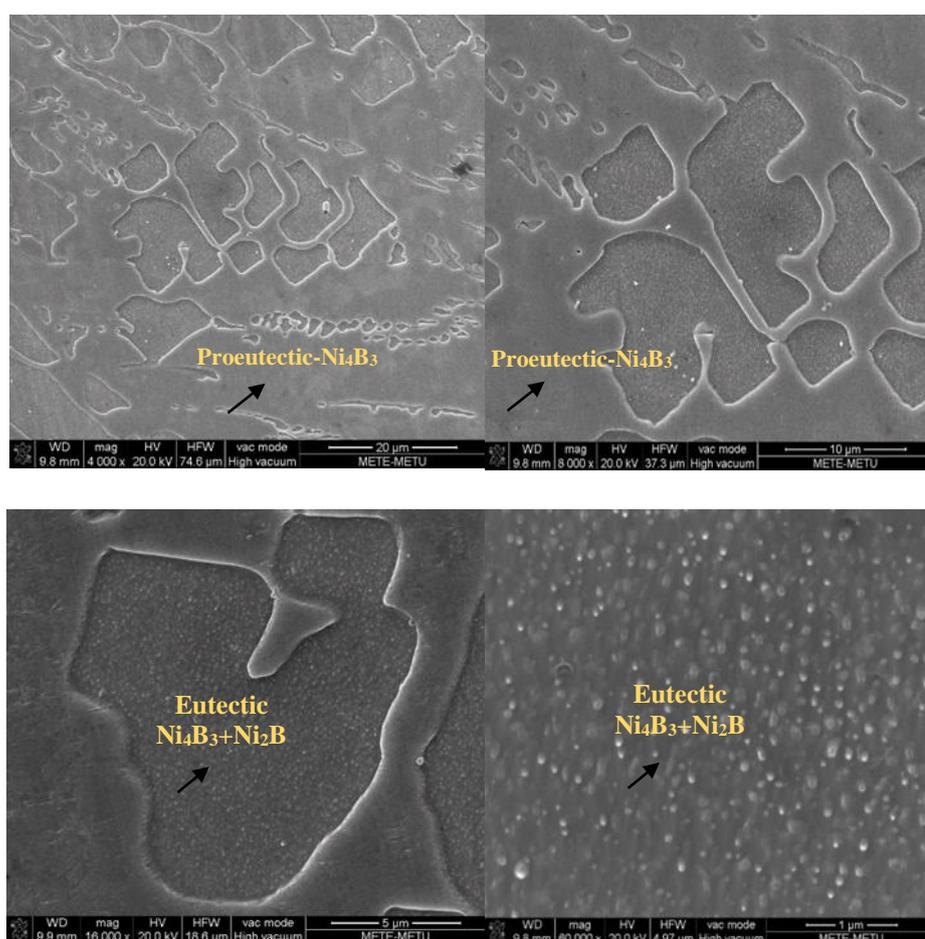
Figure 4.2 SEM images of $Ni_{60}B_{40}$ bulk alloys showing pro-eutectic and eutectic intermetallic phases

EDS analysis shown in the Fig. 4.3 proves the presence of Ni_2B and Ni_4B_3 phases in the alloy. Thermal behavior of $Ni_{60}B_{40}$ bulk alloys have been analyzed by means of differential scanning calorimeter (DSC), Figure 4.5, from which the melting

temperatures of the phases Ni_4B_3 and Ni_2B have been determined as 1025°C and 1142°C, respectively, which coincide well with data published in the literature [34].

Element	Wt%	At%
Ni	91	65
B	9	35

Element	Wt%	At%
Ni	89	61
B	11	39

Element	Wt%	At%
Ni	86	54
B	14	46
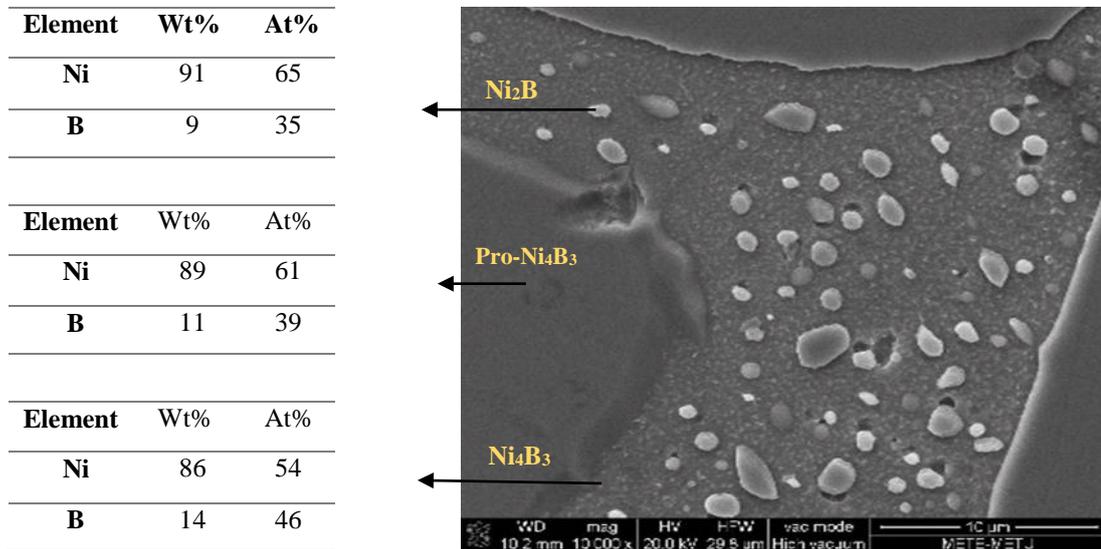
Figure 4.3 EDS results of $Ni_{60}B_{40}$ bulk alloys
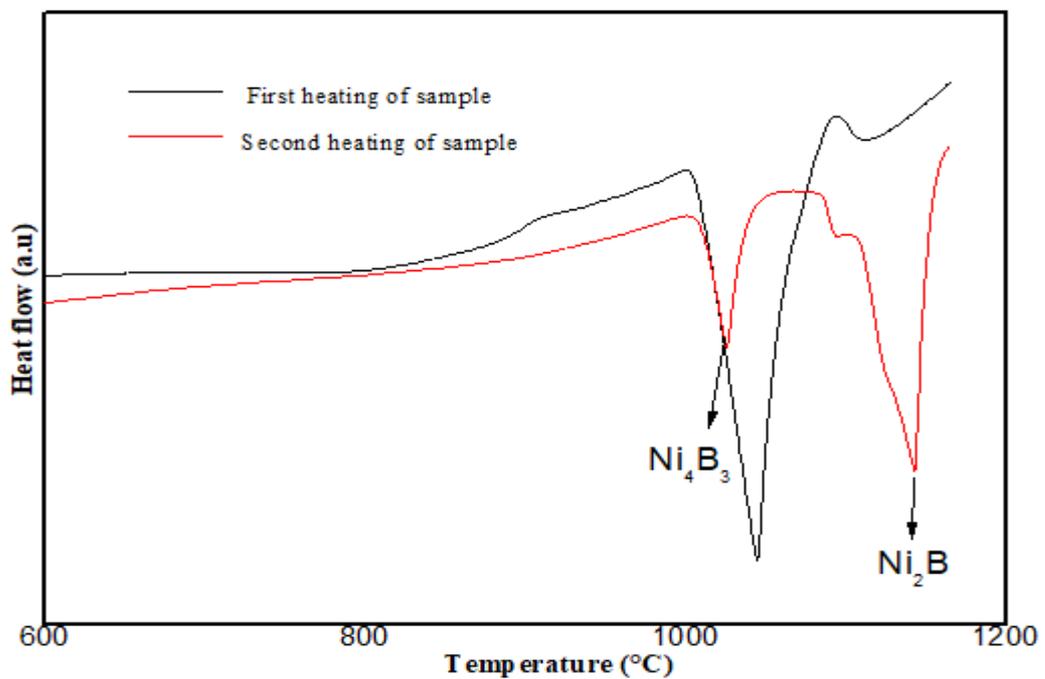
Figure 4.4 DSC analysis of the $Ni_{60}B_{40}$ bulk alloys

33

Figure 4.5 shows the hysteresis curves for the $Ni_{60}B_{40}$ bulk alloy. As the magnetic field is applied to bulk $Ni_{60}B_{40}$ alloy hysteresis loop is obtained and saturation magnetization occurs. The area of hysteresis loop is associated with the amount of energy dissipation upon reversal of the field and a narrow hysteresis is a sign of existing a small amount of energy dissipation which is used in transformer and motor cores.
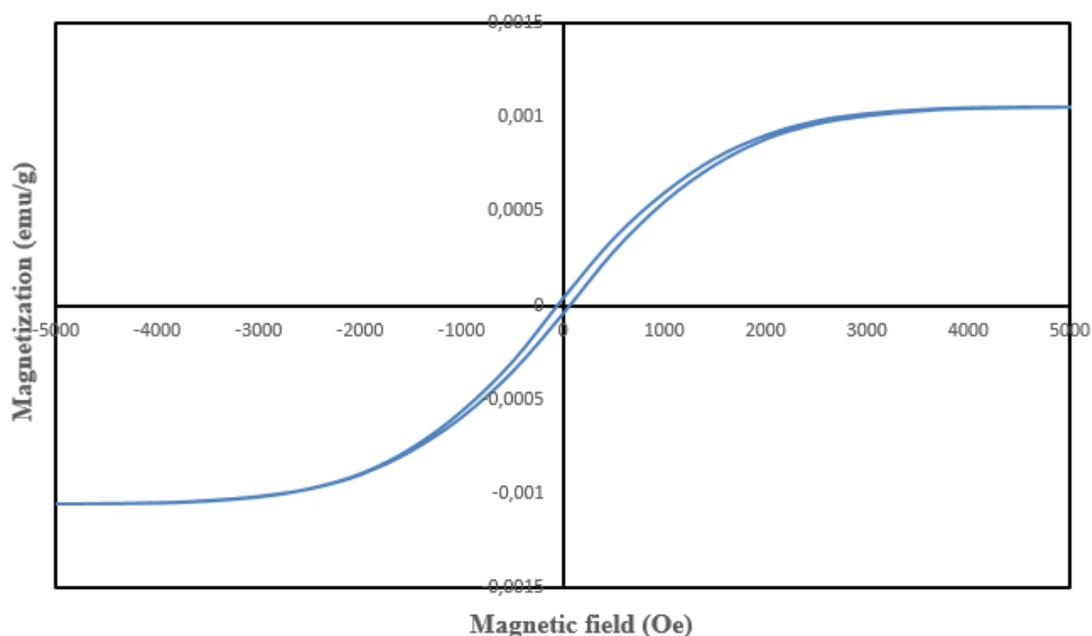
Figure 4.5 Hysteresis curves for $Ni_{60}B_{40}$ bulk alloys

Furthermore, some magnetic parameters including Ms (saturation mag.), Mr (remanent mag.), S (squareness) and Hc (coercivity) were calculated and given in Table 4.1.

Table 4.1 Magnetic properties of $Ni_{60}B_{40}$ bulk alloys

Saturation Mag., Ms, (emu/g)	1.66×10^{-2}
Remanent Mag., Mr, (emu/g)	6.47×10^{-4}
Squareness, S, (Mr/Ms)	3.89×10^{-2}
Coercivity, Hc, (Oe)	61.22

4.2. Characterization of pure Ni powders

Figure 4.6 shows the XRD curves of the unmilled and milled pure nickel powders for different time periods. As known, Ni has a face centered cubic (FCC) crystal structure; Ni peaks indicated confirms the FCC crystal structure in terms of the Miller indices rule that all indices should be either even or odd. The diffraction peaks of Ni were indexed as (111), (200), (220), (311) and (222), respectively.
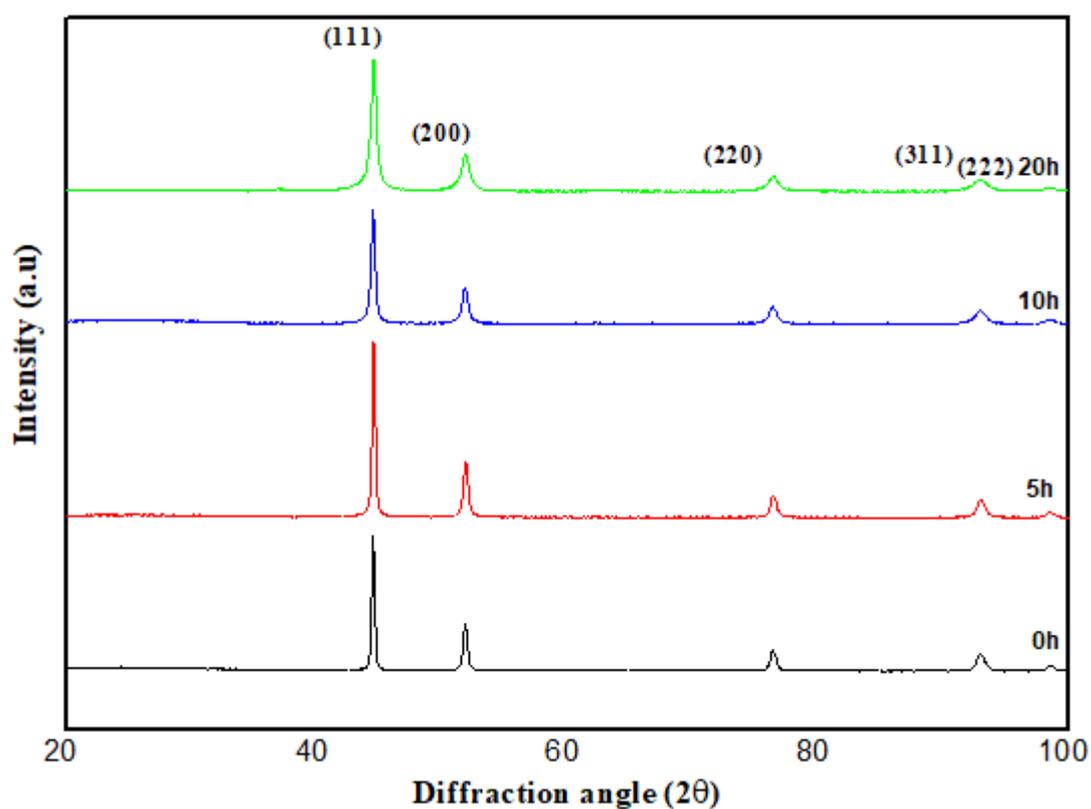
Figure 4.6 X-Ray diffraction patterns for unmilled and milled pure Ni powders for different time periods.

The milling process was completed after 20 hours of milling time. Neither additional peaks (oxidation, impurity etc.) nor shift of existing peaks toward the other angles are observed in the diffractograms.

Another result obtained from the diffractograms is that, peak broadening increases with the further milling times. Decreasing of the crystallite size during the milling process explains the reason of increasing peak broadening. Figure 4.7 shows the detail view of diffraction peak (111) for the unmilled and milled Ni powders
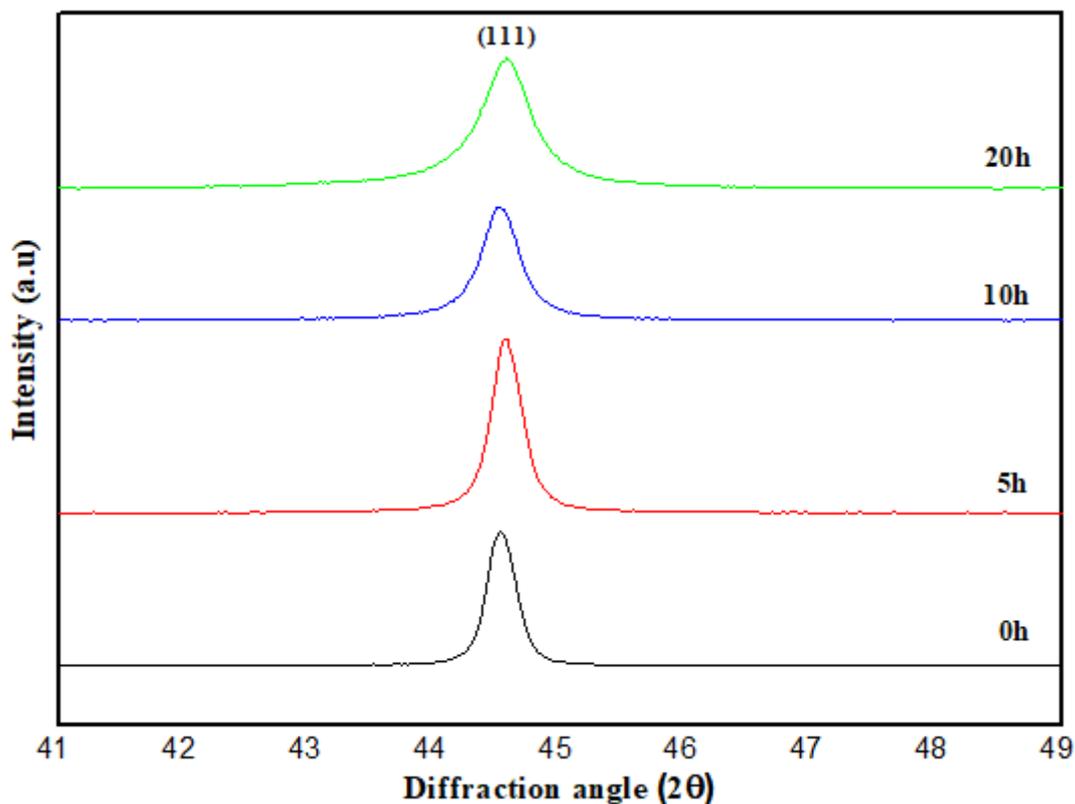

Figure 4.7 X-Ray diffraction peak of (111) for unmilled and milled pure Ni powders for different time periods

With the help of (111) peak, crystallite sizes of Ni were calculated by using Scherrer equation shown in below;

$$t = \frac{0.9\,\lambda}{\beta\,\cos(\theta)} \qquad\qquad \text{Equation 1}$$

In this equation t is the crystallite size, λ is the x-ray wavelength, β is the line broadening at half the maximum intensity (FWHM) of the (111) peak, and Θ is the Bragg angle. Table 4.2 shows the crystallite sizes of the Ni powders, calculated by the Scherrer equation for different milling time periods.

Table 4.2 The crystallite sizes of Ni, calculated by the Scherrer equation for different milling time periods

Milling time (h)	Crystallite sizes (nm)
0	25.84 ± 2.5
5	21.83 ± 2.18
10	16.73 ± 1.67
20	11.72 ± 1.17

After milling process, particle morphology (spherical, cubic, stick, etc.), size and distribution were examined by Scanning Electron Microscopy (SEM). It can be obtained from the SEM images of the unmilled and milled pure plate shaped Ni powders shown in Figure 4.8 that particle size whose average is equal to 62.96 µm for unmilled Ni powders has been reduced down to average 812.64 nm at the end of the milling process.
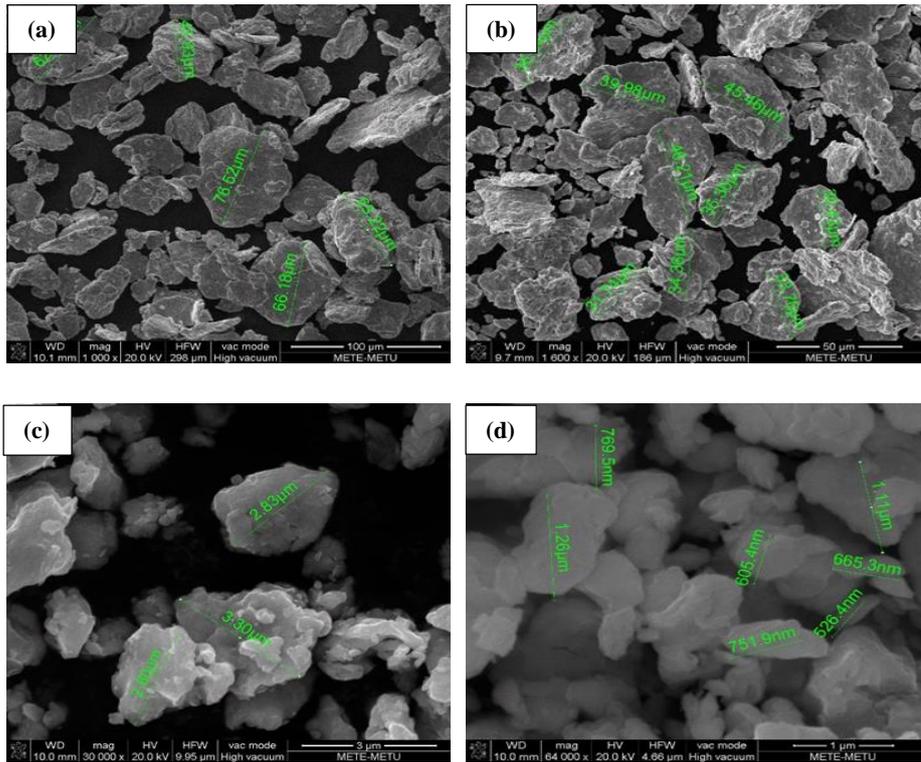
Figure 4.8 SEM images of (a) unmilled pure Ni powders and powders milled for

(b) 5 h, (c) 10 h, (d) 20 h

4.3. Characterization of Ni$_{60}$B$_{40}$ nanoalloys

After understanding mechanism of high energy ball milling by grinding pure Ni powders as well as characterization of them, Ni$_{60}$B$_{40}$ composition powders were prepared then subjected to milling process up to 80 hours of milling time. After certain intervals, the process was interrupted and powders were received from the bowls for characterization. XRD analysis of the unmilled and milled Ni$_{60}$B$_{40}$ powders at certain intervals are shown in Figure 4.9.
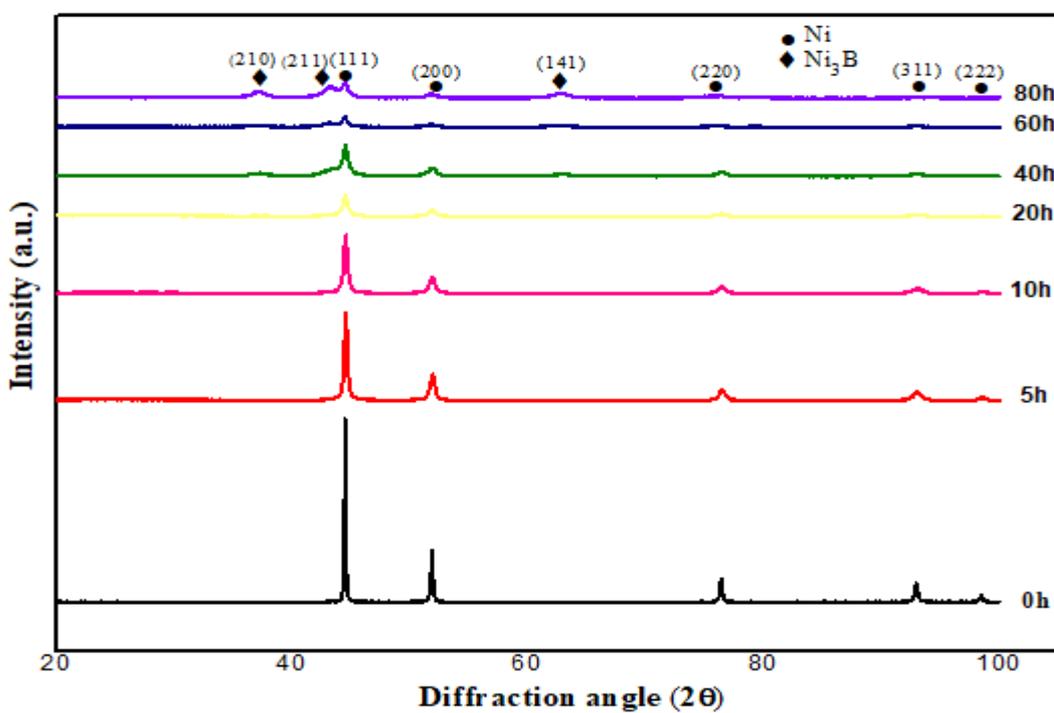
Figure 4.9 X-Ray diffraction patterns of $Ni_{60}B_{40}$, initial powders and powders ball milled for 5, 10, 20, 40, 60 and 80 h
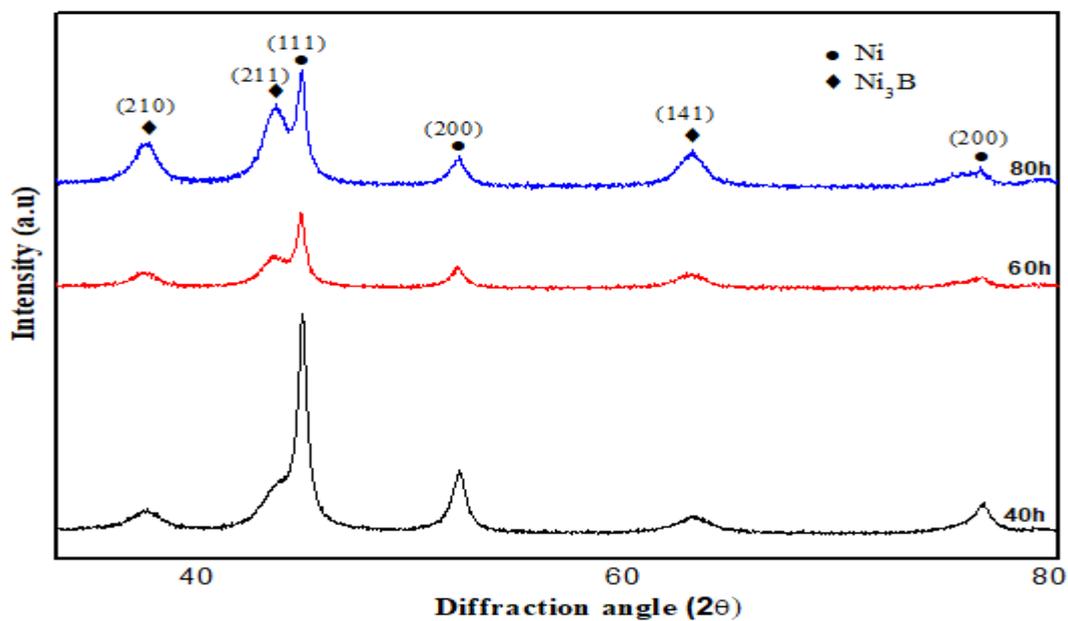
Figure 4.10 X-Ray diffraction patterns of $Ni_{60}B_{40}$ nanoalloys in detail for 40, 60 and 80 h milling times

It can be seen from the XRD pattern of the $Ni_{60}B_{40}$ nanoalloy powders depicted in Figure 4.10 for different milling time periods that intensity of the (111), (200), (220), (311), (222) Ni peaks decrease with increasing milling times and (222) Ni peak disappears after completion of the 80 hours of milling time. Broadening of the existing peaks depicted in Figure 4.11 was also evident for decrease in crystallite sizes. Furthermore, before 40 hours of milling time neither shift of existing peaks toward the lower angles nor additional peaks centered at other angles are observed. However; after 40 hours of milling time Ni_3B intermetallic crystalline phase having orthorhombic crystal structure which was indexed as (210), (211) and (141) have been detected and the intensity of peaks increases with further increases of milling time. The reason behind this increment is the increase of the amount of Ni_3B phase.

With the help of XRD analysis, crystallite size of the unmilled and milled $Ni_{60}B_{40}$ nanoalloy powders shown in Table 4.3 were calculated by the Scherrer equation (Eq. 1). According to results, crystallite size of the unmilled $Ni_{60}B_{40}$ powders measured as 24.88 ± 2.48 nm have been reduced down to 8.78 ± 0.87 nm after 80 hours of milling time.

Table 4.3 The crystallite sizes of $Ni_{60}B_{40}$ powders, calculated by the Scherrer equation for different milling time periods

Milling time (h)	Crystallite sizes (nm)
0	24.88 ± 2.48
5	21.88 ± 2.18
10	19.25 ± 1.92
20	13.81 ± 1.38
40	12.75 ± 1.27
60	12.14 ± 1.21
80	8.78 ± 0.87

For examination of particle morphology (cubic, spherical, plate like, etc.) and particle size, scanning electron microscopy (SEM) analysis shown in Figure 4.11 was applied.
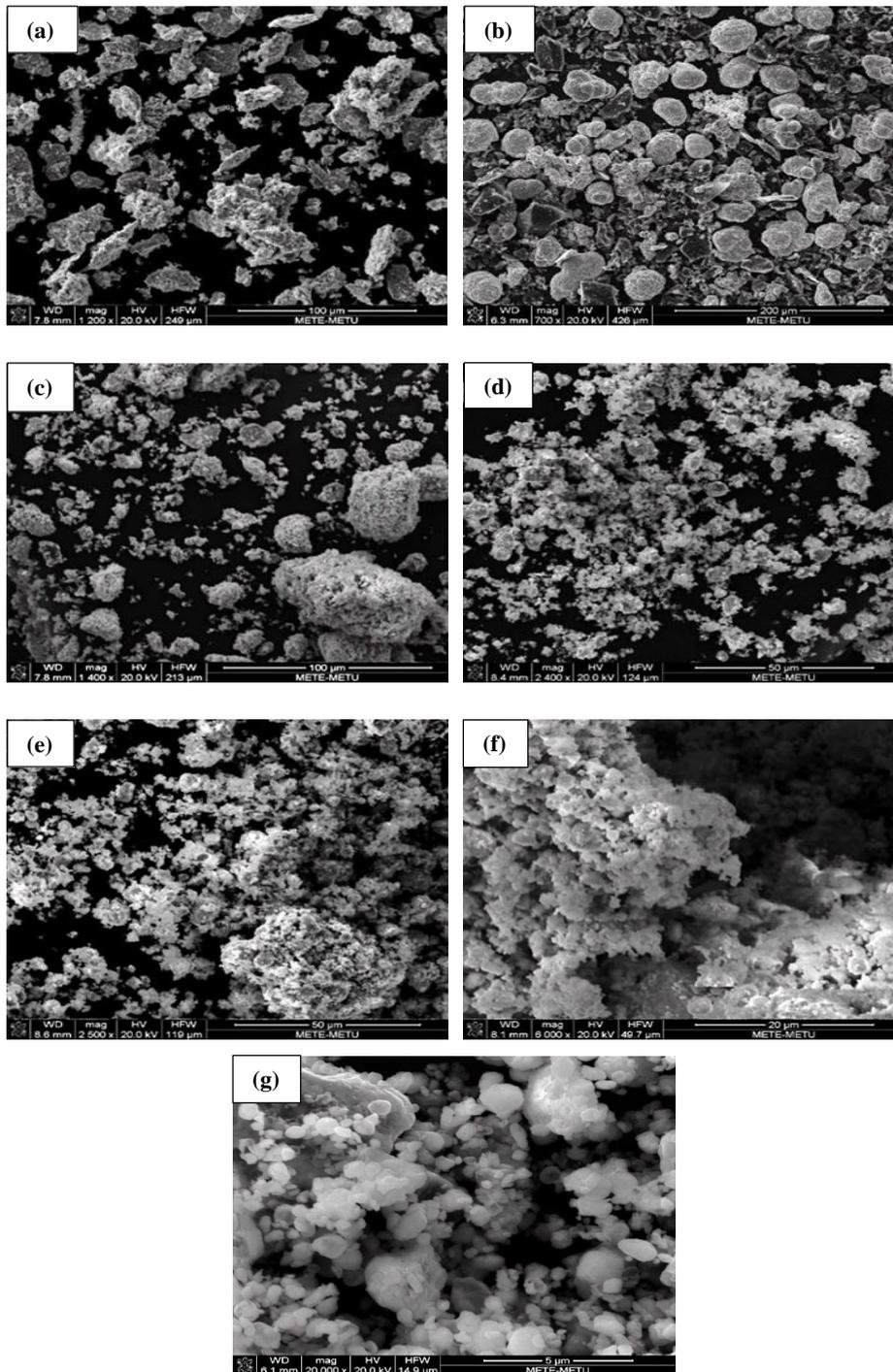
Figure 4.11 SEM images for $Ni_{60}B_{40}$ composition powder milled for (a) 0 h (initial),
(b) 5 h, (c) 10 h, (d) 20 h, (e) 40 h, (f) 60 h, (g) 80 h

It can be understood from the SEM images that spherical (Ni) and plate (B) shaped particles become deformed with longer milling times. Additionally, particle sizes were measured for all milling time periods and initial sub-micron sized particles have been reduced down to a size ranged in between 50-100 nm at the end of ball milling procedure which is shown in Figure 4.12. Average particle size of the milled particles was calculated as 91.01 nm.
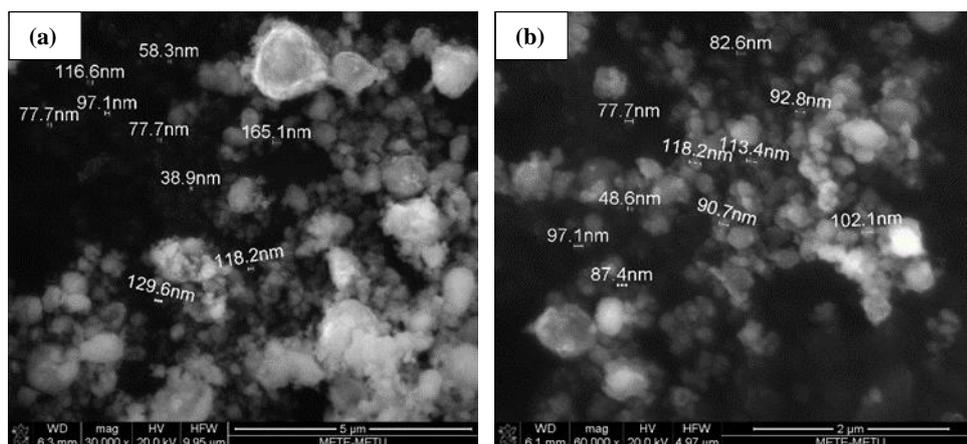
Figure 4.12 High Resolution SEM images for $Ni_{60}B_{40}$ composition powder milled (a) 60 h (b) 80 h

DSC analysis was carried out to analyze thermal behavior of nanoalloys. Figure 4.13 shows the DSC curves of powder samples for 80 h milling time. It is evident that, nanoalloy powders shows the amorphization behavior and glass transition and crystallization temperatures determined from the curves as 388 °C and 502 °C, respectively. At the end of the ball milling operation, it can be understood from the XRD and DSC curves that, the structure is composed of an amorphous matrix, nanocrystalline Ni particles having interstitial B atoms and Ni_3B crystalline phase.
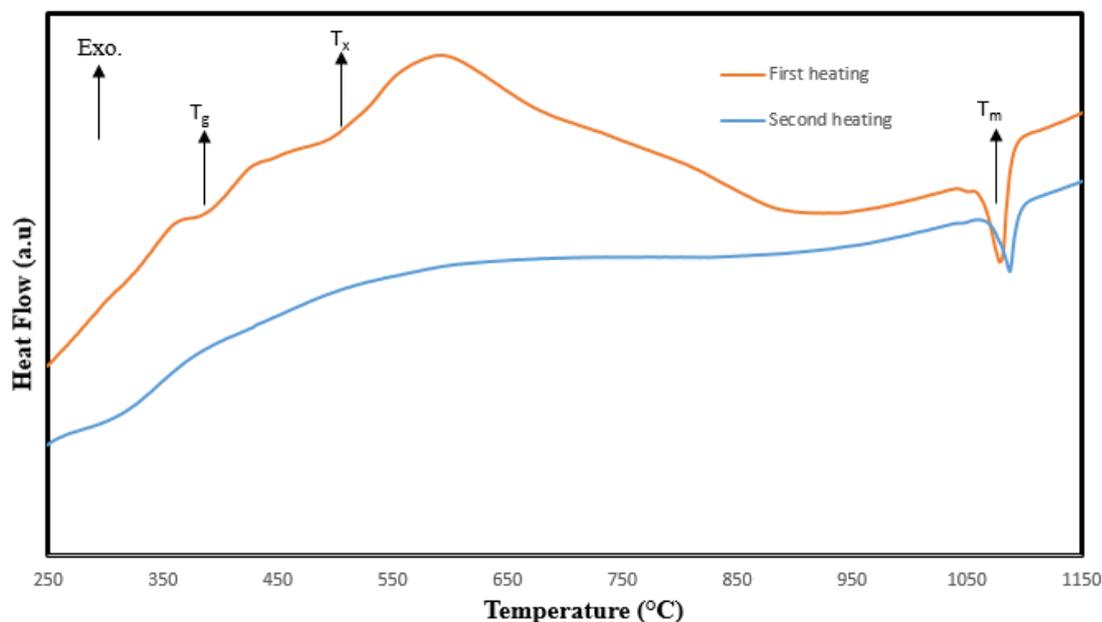
Figure 4.13 DSC analyses of the milled $Ni_{60}B_{40}$ powder for 80 h

High temperature XRD analysis was applied to 60 hours milled $Ni_{60}B_{40}$ nanoalloys to verify the stable phases at the end of process. The temperatures were determined from DSC curves of the 60 hours milled $Ni_{60}B_{40}$ nanoalloys. Metastable phases disappeared with the increasing temperature and the phase stability was provided at 800 °C. Ni_4B_3 and Ni_3B have been detected as stable phases. The figure which is below shows the High Temperature XRD pattern of the 60 h milled $Ni_{60}B_{40}$ at 800 °C.
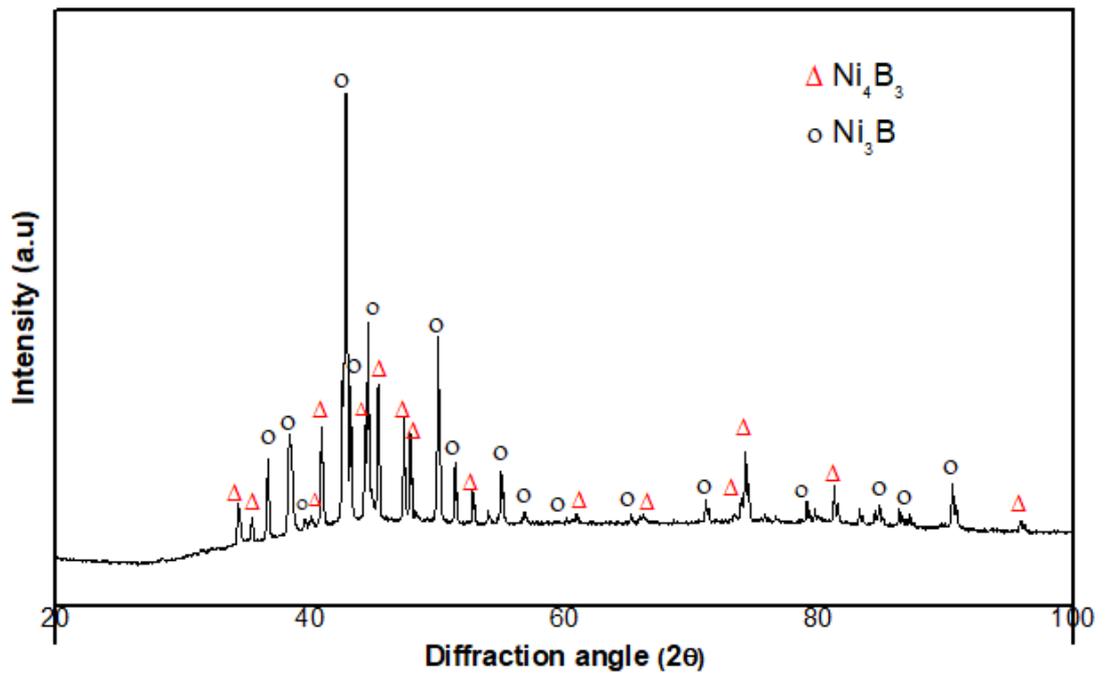
Figure 4.14 High temperature XRD pattern of the 60 h milled $Ni_{60}B_{40}$ at 800 °C.

VSM analysis was applied to examine the magnetic behavior of unmilled and milled $Ni_{60}B_{40}$ powders for different time periods. Hysteresis curves of the unmilled and milled $Ni_{60}B_{40}$ nanoalloy powders shown in Figure 4.15 were attained through the VSM analysis for different milling time periods. Furthermore, magnetic parameters of the unmilled and milled $Ni_{60}B_{40}$ powders obtained from hysteresis curves are shown in Table 4.4.
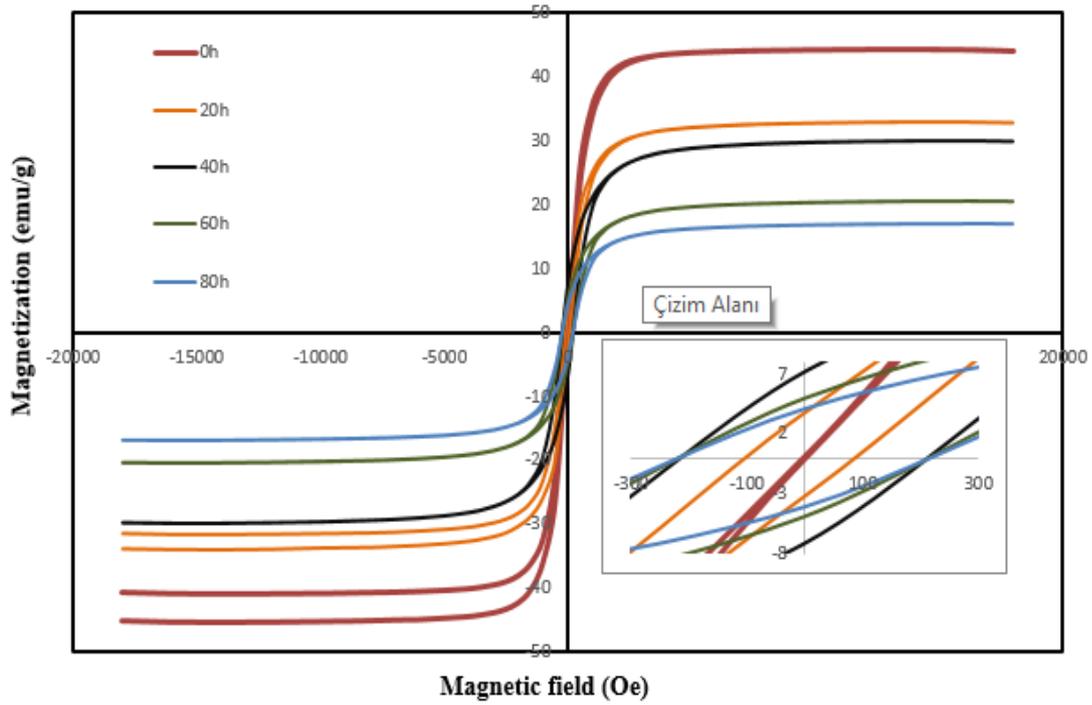
Figure 4.15 Hysteresis curves for initial $Ni_{60}B_{40}$ powder and powders milled for different time periods

Table 4.4 Magnetic properties of initial $Ni_{60}B_{40}$ powder and powders milled for different time periods

Milling time (h)	Saturation Mag., Ms, (emu/g)	Remanent Mag., Mr, (emu/g)	Squareness, S, (Mr/Ms)	Coercivity, Hc, (Oe)
0	44.8	0.1	0.002	2.261
20	33.3	3.48	0.104	95.213
40	29.9	7.13	0.239	209.818
60	20.4	4.91	0.24	212.393
80	16.9	4.08	0.241	213.201

As seen in Table 4.4 powders milled for different time periods displayed soft magnetic behavior with high saturation magnetization and high initial permeability. With the increasing of milling time while saturation magnetization values decreased, but coercivity values increased. As can be deduced from the electron microscopy images, nano-particle size became smaller and at the same time their proportion, i.e. number of nano-size particles increased in $Ni_{60}B_{40}$ nanoalloy powder with increasing milling time. Furthermore, according to SEM, XRD and DSC results, at 40 h of milling time amorphous phase started to form and nanoalloy powder can be considered as a composite, consisting of Ni-B amorphous phase and FCC-Ni(B) and Ni_3B crystalline phases. The decrease in saturation magnetization and increase in coercivity values can be attributed to the existence of such a composite structure in $Ni_{60}B_{40}$ nanoalloy powder. Given the fact that there are no magnetic domains in glassy magnetic materials the "barrier" changes against magnetization is very low.

CHAPTER 5

CONCLUSIONS AND FUTURE WORKS

5.1. Conclusions

In this thesis, $Ni_{60}B_{40}$ alloys have been successfully synthesized, in the bulk and nanocrystalline/amorphous forms by means of arc melting and water cooled copper mold casting methods under controlled atmosphere and high energy ball milling technique, respectively. Then, comparable characterization of them in term of crystalline structure, microstructure, morphology and size of nanoparticles, as well as magnetic properties have been provided by means of X-ray diffractometer, SEM-EDS, DSC and VSM characterization techniques.

Initially, bulk $Ni_{60}B_{40}$ alloys were produced in equilibrium and non-equilibrium casting conditions and presence of two Ni_4B_3 and Ni_2B intermetallic phases were detected by X-ray diffractometer, SEM-EDS and DSC analysis. On the base of DSC analysis, the melting temperatures of the Ni_4B_3 and Ni_2B phases have been determined as 1025°C and 1142°C, respectively, which coincide well with data published in the literature.

After the completing of structural characterization of $Ni_{60}B_{40}$ bulk alloy, milling operation was carried out with Ni and B powders. They have been milled for 5, 10, 20, 40, 60 and 80 hours of milling time and certain amount of specimens was received from the bowls at determined milling times for characterization. In order to preclude oxidation during milling, Argon inert gas was transferred into bowls before milling started. Initial sub-micron sized particles have been reduced down to a size ranged in between 50-100 nm at the end of ball milling procedure. It is shown that, microstructure of $Ni_{60}B_{40}$ nanoalloys strongly depend on milling time; amorphization of alloy starts at 40 h milling time and Ni_3B intermetallic phase starts to form at 60 h

and grow with further increasing of milling time. DSC analysis of nanoalloy powders milled for 80 h milling time reveal that the $Ni_{60}B_{40}$ nanoalloys show an amorphization behavior and glass transition and crystallization temperatures have been determined as 388 °C and 502 °C, respectively. Also, in terms of the particle size, according to SEM analyses, with increasing of milling time, average particle size decreases and number of sub-micron particles increases with increasing milling time.

Magnetic properties of $Ni_{60}B_{40}$ bulk and nanoalloy powders have been measured by using vibrating-sample magnetometer (VSM). VSM analysis indicates that $Ni_{60}B_{40}$ bulk alloys show a soft magnetic property, having 1.66×10^{-2} emu/g saturation magnetization and 61.22 Oe coercivity values. However, magnetic measurements for $Ni_{60}B_{40}$ nanoalloy powders reveal that there is a general decrease in saturation magnetization and increase in coercivity with the further increases of milling time. Consequently, with the increasing of milling time, ferromagnetism become more effective for $Ni_{60}B_{40}$ nanoalloy.

5.2. Future Works

For further research:

- More experimental investigations might be performed in order to synthesize Ni-B nanopowders having different compositions and smaller particle size with enhanced structural and physico-chemical properties by varying ball milling process parameters, i.e. rotating speed, cycle intervals, bowl and ball type and their sizes, milling speeds and milling times, etc.

- Modeling and computer simulation studies would be carried out to obtain a relationship between the structural, magnetic and electronic properties of Ni-B nanoalloys.

- Theoretical studies could be done according to Ni-B binary system and also comparison between experimental results and theoretical predictions can be provided.

- Furthermore, the Transition Electron Microscopy (TEM) analysis would be utilized for better analysis of structural evolution in Ni-B nanoalloys, i.e. changes in nanoparticles morphologies, shape and size distribution with variation of ball milling time.

REFERENCES

[1]   R. Ferrando, J. Jellinek, and R. L. Johnston, "Nanoalloys: From theory to applications of alloy clusters and nanoparticles," Chem. Rev., vol. 108, no. 3, pp. 845–910, 2008.

[2]   D. Alloyeau, C. Mottet, and C. Ricolleau, Eds., Nanoalloys: Synthesis, Structure and Properties. London: Springer, 2012.

[3]   R. Fernando, Structure and Properties of Nanoalloys, 10th ed. Elsevier Ltd, 2016.

[4]   A. Mohajeri, "Mg/Cu bimetallic nanoalloys: Morphologies, electronic structures, and catalysis of O2dissociation," J. Alloys Compd., vol. 735, pp. 1962–1970, 2018.

[5]   U. Kreibig and M. Vollmer, Optical Properties of Metal Clusters, 1st ed. Berlin: Springer, 1995.

[6]   G. Rossi, A. Rapallo, C. Mottet, A. Fortunelli, F. Baletto, and R. Ferrando, "Magic polyicosahedral core-shell clusters," Phys. Rev. Lett., vol. 93, no. 10, pp. 1–4, 2004.

[7]   J. A. Blackman, "Metallic Nanoparticles," Handb. Met. Phys., vol. 5, pp. 175–229, 2008.

[8]   A. V. Ruban, H. L. Skriver, and J. K. Nørskov, "Surface segregation energies in transition-metal alloys," Phys. Rev. B - Condens. Matter Mater. Phys., vol. 59, no. 24, pp. 15990–16000, 1999.

[9]   M. Sansa, F. Ribeiro, A. Dhouib, and G. Tréglia, "Effect of magnetism on surface segregation in FeNi alloys," J. Phys. Condens. Matter, vol. 28, no. 6, 2016.

[10]   J. Blackman, Ed., Metallic Nanoparticles, 1st ed. Elsevier, 2009.

[11]   T. Shibata, B. A. Bunker, Z. Zhang, D. Meisel, C. F. Vardeman, and J. D. Gezelter, "Size-dependent spontaneous alloying of Au-Ag nanoparticles," J. Am. Chem. Soc., vol. 124, no. 40, pp. 11989–11996, 2002.

[12]   Z. Peng and H. Yang, "Ag-Pt alloy nanoparticles with the compositions in the miscibility gap," J. Solid State Chem., vol. 181, no. 7, pp. 1546–1551, 2008.

[13]   B. Reddy, S. Nayak, S. Khanna, B. Rao, and P. Jena, "Electronic structure and magnetism of Rhn (n=2–13) clusters," Phys. Rev. B, vol. 59, no. 7, pp. 5214–5222, 1999.

[14]   A. M. Molenbroek, S. Haukka, and B. S. Clausen, "Alloying in Cu/Pd Nanoparticle Catalysts," J. Phys. Chem. B, vol. 102, no. 52, pp. 10680–10689, 1998.

[15]   J. Tersoff, "Kinetic surface segregation and the evolution of nanostructures," Appl. Phys. Lett., vol. 83, no. 2, pp. 353–355, 2003.

[16]   G. Barcaro, A. Fortunelli, G. Rossi, F. Nita, and R. Ferrando, "Electronic and structural shell closure in AgCu and AuCu nanoclusters," J. Phys. Chem. B, vol. 110, no. 46, pp. 23197–23203, 2006.

[17]   C. Rajesh and C. Majumder, "Energy level reordering and stability of MPb_{12} clusters: An interplay between geometry and electronic structure," Chem. Phys. Lett., vol. 430, no. 1–3, pp. 101–107, 2006.

[18]   G. Schmid, H. West, J. Malm, J. Bovin, and C. Grenthe, "Catalytic properties of layered Gold- Palladium Colloids," Inorg. Chem., vol. 2, no. 9, pp. 1099–1103, 1996.

[19]   G. J. Hutchings and C. J. Kiely, "Strategies for the synthesis of supported gold palladium nanoparticles with controlled morphology and composition," Acc. Chem. Res., vol. 46, no. 8, pp. 1759–1772, 2013.

[20]   L. Piccolo et al., "Understanding and controlling the structure and segregation behaviour of AuRh nanocatalysts," Sci. Rep., vol. 6, no. June, pp. 1–8, 2016.

[21]   R. Raja et al., "Highly efficient catalysts for the hydrogenation of nitro-substituted aromatics.," Chem. Commun., no. 15, pp. 2026–2028, 2005.

[22]   T. Toda, "Enhancement of the electroreduction of Oxygen on Pt alloys with Fe, Ni, and Co," J. Electrochem. Soc., vol. 146, no. 10, p. 3750, 1999.

[23]   R. S. Sundar and S. C. Deevi, Soft magnetic FeCo alloys: alloy development, processing, and properties, vol. 50, no. 3. 2005.

[24]   W. S. Seo et al., "FeCo/graphitic-shell nanocrystals as advanced magnetic-resonance-imaging and near-infrared agents," Nat. Mater., vol. 5, no. 12, pp. 971–976, 2006.

[25]   Q. Wong and Y. Li, "Fabrication of soft magnetic Fe-based nanoalloy."

[26]   K. McNamara and S. A. M. Tofail, "Nanoparticles in biomedical applications," Adv. Phys. X, vol. 2, no. 1, pp. 54–88, 2017.

[27]   K. S. Kumar, H. Van Swygenhoven, and S. Suresh, "Mechanical behavior of nanocrystalline metals and alloys," Acta Mater., vol. 51, no. 19, pp. 5743–5774, 2003.

[28]   J. R. Davis, ASM Specialty Handbook: Nickel, Cobalt, and their alloys. 2000.

[29]   O. Teppa and P. Taskinen, "Thermodynamic assessment of Ni–B phase diagram," Mater. Sci. Technol., vol. 9, no. 3, pp. 205–212, 1993.

[30]   J. Diabb, A. Juárez-Hernandez, R. Colas, A. G. Castillo, E. García-Sanchez, and M. A. L. Hernandez-Rodriguez, "Boron influence on wear resistance in nickel-based alloys," Wear, vol. 267, no. 1–4, pp. 550–555, 2009.

[31]   L. Xi et al., "Investigation of Ni-B alloys for joining of TiB_2 ultra-high-temperature ceramic," J. Mater. Eng. Perform., vol. 25, no. 8, pp. 3204–3210, 2016.

[32]   F. Mindivan, H. Mindivan, and C. Darcan, "Electroless Ni–B coating of pure titanium surface for enhanced tribocorrosion performance in artificial saliva and antibacterial activity," Tribol. Ind., vol. 39, no. 2, pp. 270–276, 2017.

[33]   F. Bülbül, H. Altun, V. Ezirmik, and Ö. Küçük, "Investigation of structural, tribological and corrosion properties of electroless Ni-B coating deposited on 316L stainless steel," Proc. Inst. Mech. Eng. Part J J. Eng. Tribol., vol. 227, no. 6, pp. 629–639, 2013.

[34]   J. a. Glass, S. Kher, Y. Kim, P. A. Dowben, and J. T. Spencer, "The Deposition of Nickel Boride Thin Films by Borane and Metallaborane Cluster Compounds," vol.204, pp. 439-444, 1990.

[35]   R. Weil and K. Parker, "Chapter 4 The properties of electroless nickel," pp. 111–137.

[36]   M. Nazarian-samani, A. R. Kamali, R. Mobarra, and M. Nazarian-samani, "Phase transformations of Ni-15 wt.% B powders during mechanical alloying and annealing," Mater. Lett., vol. 64, no. 3, pp. 309–312, 2010.

[37]   A. V Paustovskii, B. M. Rud, E. Y. Tel, A. I. Vlasenko, V. E. Shelud, and A. B. Smirnov, "Theory and technology of sintering, heat and chemical heat treatment processes laser treatment of thick films based on powder composites of nickel boride," vol. 41, no. 424, pp. 119–122, 2002.

[38]   Y. W. Riddle and T. O. Bailer, "Friction and wear reduction via an Ni-B electroless bath coating for metal alloys," 2005.

[39]   V. Vitry and L. Bonin, "Formation and characterization of multilayers borohydride and hypophosphite reduced electroless nickel deposits," Electrochem. Acta, 2017.

[40]   X. Feng, Y. Bai, Y. Zhao, J. Yang, J. Chi, and L. Bo, "Synthesis of nanocrystalline Ni_2B via a solvo-thermal route," vol. 7, pp. 189–191, 2004.

[41]   B. Hong, Z. Peng, and S. Suda, "Nickel and cobalt based catalysts for hydrogen generation by hydrolysis of borohydride," vol. 415, pp. 288–293, 2006.

[42]   S. Rundqvist et al., "Crystal structure refinements of Ni$_3$B, o-Ni$_4$B$_3$, and m-Ni$_4$B$_3$.," Acta Chemica Scandinavica, vol. 21. pp. 191–194, 1967.

[43]   S. Diplas, J. Lehrmann, S. Jorgensen, T. Valand, J. F. Watts, and J. Taft, "Characterization of Ni-B amorphous alloys with x-ray photoelectron and secondary ion mass spectroscopy," Surf. Interface Anal., vol. 37, no. 5, pp. 459–465, 2005.

[44]   A. Inoue, A. Kitamura, and T. Masumoto, "Ni-B and Co-B amorphous alloys with high boron concentration," 1979.

[45]   A. N. Campbell, J. C. Barbour, C. R. Hills, and M. Nastasi, "The formation of amorphous Ni-B by solid state and ion-beam reaction," J. Mater. Res., vol. 4, no. 6, pp. 1303–1306, 1989.

[46]   H. Li, H. Li, W. Dai, and M. Qiao, "Preparation of the Ni-B amorphous alloys with variable boron content and its correlation to the hydrogenation activity," Appl. Catal. A Gen., vol. 238, no. 1, pp. 119–130, 2002.

[47]   Y. Wang et al., "Hydrogen storage in a Ni–B nanoalloy-doped three-dimensional graphene material," Energy Environ. Sci., vol. 4, no. 1, pp. 195–200, 2011.

[48]   F. Taghavi, C. Falamaki, A. Shabanov, M. Seyyedi, and M. Zare, "An effective method for increasing the activity of nickel boride catalyst nano-particles in hydrogenation reactions: Low-temperature hydrogen treatment," Appl. Catal. A Gen., vol. 453, pp. 334–340, 2013.

[49]   C. H. Du, Y. Zhao, and D. Sun, "A Co-promoted Ni-B amorphous nanoalloy catalyst for liquid phase hydrogenation of furfural to furfural alcohol," Environ. Biotechnol. Mater. Eng. Pts 1-3, vol. 183–185, pp. 2322–2326, 2011.

[50]   G. Bai, H. Dong, Z. Zhao, Y. Wang, Q. Chen, and M. Qiu, "Preparation of nanoscale Ni–B amorphous alloys and their application in the Selective Hydrogenation of Cinnamic Acid," J. Nanosci. Nanotechnol., vol. 13, no. 7, pp. 5012–5016, 2013.

[51]   J. Guo, Y. Hou, B. Li, and E. Duan, "Morphology-controlled synthesis of Ni-B nanoparticles by addition of hydrogen peroxide," Mater. Lett., vol. 200, pp. 90–93, 2017.

[52]   F. M. F. Rhen, D. Richardson, C. A. D. Pomar, and J. A. Souza, "Investigation of Magnetic Properties of Ni – B Nanotubes at Low Temperatures," vol. 52, no. 5, pp. 10–13, 2016.

[53]   S. Wei et al., "X-ray-absorption fine structure study on devitrification of ultrafine amorphous Ni-B alloys," vol. 63, pp. 1–5, 2001.

[54]	M. Wen, L. Li, Q. Liu, H. Qi, and T. Zhang, "The preparation of well-dispersed Ni–B amorphous alloy nanoparticles at room temperature," vol. 455, pp. 510–515, 2008.

[55]	Y. Wang, J. Liu, K. Wang, T. Chen, X. Tan, and C. M. Li, "Hydrogen storage in Ni-B nanoalloy-doped 2D graphene," Int. J. Hydrogen Energy, vol. 36, no. 20, pp. 12950–12954, 2011.

[56]	F. Taghavi, C. Falamaki, A. Shabanov, L. Bayrami, and A. Roumianfar, "Applied Catalysis A: General Kinetic study of the hydrogenation of p-nitrophenol to p-aminophenol over micro-aggregates of nano-Ni$_2$B catalyst particles," "Applied Catal. A, Gen., vol. 407, no. 1–2, pp. 173–180, 2011.

[57]	H. Kwon, K. Kim, H. Ahn, and Y. Kim, "Electrodeposition and characterization of nanocrystalline Ni–B with low boron content for MEMS Applications," vol. 29, no. 3, pp. 225–234, 2017.

[58]	L. Xu, J. Peng, B. Meng, W. Li, B. Liu, and H. Luo, "Microscale interface synthesis of Ni-B amorphous nanoparticles from NiSO$_4$ by sodium borohydride reduction in microreactor," vol. 35, no. 8, pp. 745–750, 2016.

[59]	Z. Jiang, H. Yang, Z. Wei, Z. Xie, W. Zhong, and S. Wei, "Catalytic properties and structures of nano-amorphous Ni – B alloys affected by annealing temperatures," vol. 279, pp. 165–171, 2005.

[60]	M. Zeng, H. Wang, C. Zhao, J. Wei, K. Qi, and W. Wang, "Nanostructured amorphous nickel boride for high efficiency electrocatalytic hydrogen evolution over a broad pH range," vol. 100084, pp. 708–712, 2016.

[61]	V. Singh, P. Banerjee, V. Srinivas, and N. H. Babu, "Structural and magnetic properties of Ni rich amorphous boride nanoparticles," vol. 259, pp. 256–259, 2011.

[62]	M. A. Korchagin, D. V. Dudina, B. B. Bokhonov, N. V. Bulina, A. V. Ukhina, and I. S. Batraev, "Synthesis of nickel boride by thermal explosion in ball-milled powder mixtures," *J. Mater. Sci.*, pp. 1–8, 2018.

[63]	A. Corrias, G. Ennas, G. Marongiu, A. Musinu, G. Paschina, and D. Zedda, "The synthesis of nanocrystalline nickel boride powders by ball milling of elemental components," Mater. Sci. Eng. A, vol. 204, no. 1–2, pp. 211–216, 1995.

[64]	S. State, A. Of, A. N. A. By, and M. Alloying, "for Materials Research, Tohoku University, Sendai 980 Japan," vol. 205, pp. 195–200.

[65]	M. N. Ali and R. Kamali, "Thermokinetic study on the phase evolution of mechanically alloyed Ni – B powders," pp. 265–269, 2012.

[66]	O. F. Materials, "Ball-milling of elemental powders compound formation and / or amorphization," vol. 26, pp. 4687–4696, 1991.

[67]   R. Jang, "Double amorphization in the Ti-AI binary system during high-energy milling," vol. 12, pp. 66–69, 1993.

[68]   A. V Osipov and I. A. Ovid, "Diffusion-Induced decay of disclinations and solid state amorphization in mechanically alloyed materials," vol. 519, pp. 517–519, 1992.

[69]   A. Inoue, "Magnetic properties of iron-base bcc alloys produced by mechanical alloying," vol. 26, pp. 4621–4625, 1991.

[70]   M. Science, "Mechanical alloying of polytetrafluoroethylene with polyethylene," vol. 13, pp. 623–628, 1994.

[71]   J. Eckert and K. Urban, vol. 26, pp. 441–446, 1991.

[72]   D. Oleszak, "Mechanical alloying a novel method for synthesis and processing," vol. 96, no. I, pp. 101–112, 1999.

[73]   F. H. Froes and C. Suryanarayana, "Nanocrystalline metals for structural applications," vol. 2, no. June, 1989.

[74]   M. Science, "Synthesis and magnetic properties of laves phase Fe_2Nb amorphous alloy," vol. 180, pp. 177–180, 2007.

[75]   B. Fultz, C. C. Ahn, S. Spooner, L. B. Hong, J. Eckert, and W. L. Johnson, "Incipient chemical instabilities of nanophase Fe-Cu alloys prepared by mechanical alloying."

[76]   N. Q. Wu, "Amorphization of Al_4C_3 by mechanical milling," vol. 6, pp. 9–11, 1997.

[77]   A. Defence and F. Acadeuo, "Low temperature annealing of ball—milled Fer162," vol. 69, pp. 475–478, 1991.

[78]   K. A. Publishers, "Elaboration of the Cu_3Si compound using a," vol. 5, pp. 3221–3226, 2000.

[79]   X. Devaux, G. Le Ca, A. Mocellin, T. Girot, and S. B, "Modeling of the phase transformation induced by ball milling in anatase TiO_2," vol. 8, pp. 139–144, 2000.

[80]   J. S. Benjamin, "Mechanical Alloying," pp. 40–49, 1976.

[81]   C. Suryanarayana, "Mechanical alloying and milling," Prog. Mater. Sci., vol. 46, no. 1–2, pp. 1–184, 2001.

[82] A. Fadaie, M. V. Akdeniz, and A. O. Mekhrabov, Synthesis and Characterization of $Fe_{80}B_{20}$ Nanoalloys Produced by Surfactant Assisted Ball Milling, Acta Physica Polonica A, vol. 125, No. 2, pp. 597-599, 2014

[83]   L. S. Mut, A. O. Mekhrabov, M. V. Akdeniz, M. M. Karatas, Production and Structural Characterization of Ni-B Nanoalloy Synthesized by Ball Milling, 18th